Screening of compounds-based on intermediate adsorption equilibrium for electrocatalytic nitrate reduction to ammonia

Chaoqun Ma[1,2], Huaifang Zhang[1,2], Jing Xia[3*], Xiaojuan Zhu[4], Kaiyu Qu[4], Fukai Feng[1,2], Sumei Han[1,2], Caihong He[1,2], Xiao Ma[1,2], Gang Lin[1,2], Wenbin Cao[1], Xiangmin Meng[3], Lijie Zhu[5], An-Liang Wang[4*], Qipeng Lu[1,2*]

[1]School of Materials Science and Engineering, University of Science and Technology Beijing, Beijing 100083, China

[2]Shunde Innovation School, University of Science and Technology Beijing, Foshan 528399, China.

[3]Key Laboratory of Photochemical Conversion and Optoelectronic Materials, Technical Institute of Physics and Chemistry, Chinese Academy of Sciences, Beijing, 100190, China.

[4]School of Chemistry and Chemical Engineering, Shandong University, Jinan 250100, China.

[5]School of Instrument Science and Opto-Electronics Engineering, Beijing Information Science and Technology University, Beijing 100192, China.

* Corresponding author.

E-mail: qipeng@ustb.edu.cn (Q.L.); alwang@sdu.edu.cn (A-L.W.); xiajing@mail.ipc.ac.cn (J.X.).

Methods

Reagents and chemicals. Chloride hexahydrate ($Co(NO_3)_2 \cdot 6H_2O$, 99%), L-antimony potassium tartrate ($C_8H_4K_2O_{12}Sb_2.3H_2O$, 99.5%), cyanamide ($CH_2N_2$, 95%), deuterium oxide (D_2O), sodium hypochlorite (NaClO), sodium nitrate ($NaNO_3$), sodium nitrite ($NaNO_2$), sodium nitrate-^{15}N ($Na^{15}NO_3$, 98.5%), ammonium-^{15}N chloride ($^{15}NH_4Cl$, 98.5%), sodium salicylate ($C_7H_6O_3Na$), nitroferricyanide (III) dihydrate ($Na_2Fe(CN)_5NO \cdot 2H_2O$), sodium citrate dehydrate ($C_6H_5Na_3O_7 \cdot 2H_2O$), para-(dimethylamino)benzaldehyde (p-$C_9H_{11}NO$), naphthylenediamine hydrochloride ($C_{12}H_{14}N_{22} \cdot 2HCl$), sulfanilamide ($C_6H_8N_2O_2S$), phosphoric acid ($H_3PO_4$) and maleic acid ($C_4H_4O_4$) were obtained from Shanghai Macklin Biochemical Co., Ltd. Ammonium chloride (NH_4Cl), hydrazine hydrate ($N_2H_4 \cdot H_2O$), hydrochloric acid (HCl), sulfuric acid (H_2SO_4) and potassium hydroxide (KOH) were purchased from Sinopharm Chemical Reagent Co., Ltd. Ketjen Black EC300J was afforded from Suzhou Sinero Technology Co., Ltd. Ethanol (C_2H_5OH) was purchased from Tianjin Fuyu Fine Chemical Co., Ltd. The deionized water (18.2 MΩ) was used in all experiments. All reagents and chemicals are used as received without further purification.

Synthesis of CoSb IMCs/C and Co NPs/C. In a typical synthesis method, a mixture of 29.1 mg $Co(NO_3)_2 \cdot 6H_2O$, 33.4 mg $C_8H_4K_2O_{12}Sb_2.3H_2O$, 150 mg CH_2N_2 and 64 mg of carbon support (i.e., Ketjen Black EC300J) was ground using an agate mortar and pestle. After being ground thoroughly, the mixture was transferred into the porcelain boat and heated in a tube furnace under an H_2/Ar atmosphere (5 vol.% H_2). After that, the sample was heated from room temperature to 900 °C with a rate of 5 °C min^{-1} and maintained for 3 h before cooling down to room temperature. The prepared sample is named as CoSb IMCs/C.

Co NPs/C were prepared using the same method as CoSb IMCs/C, but without adding

$C_8H_4K_2O_{12}Sb_2.3H_2O$.

Material characterizations. X-ray diffraction (XRD) patterns were collected using a Bruker D8 X-ray diffractometer operating at 40 kV and 40 mA with Cu Kα radiation (λ= 1.54 Å). The microstructures and morphologies of the prepared samples were obtained by scanning electron microscopy (SEM, Hitachi S-4800) and Transmission electron microscopy (TEM, JEOL JEM-2100F). For atomic-level characterization of the prepared samples, aberration-corrected high-angle annular dark-field scanning transmission electron microscope (HAADF-STEM) and STEM energy-dispersive X-ray spectroscopy (STEM-EDS) elemental mapping images were performed on a JEOL ARM 300F (JEOL, Tokyo, Japan) operated at 300 kV equipped with a JEOL ETA corrector and an SDD-type EDS detector with the attainable energy resolution of 133 eV. X-ray photoelectron spectroscopy (XPS) measurements were determined by a Thermo Scientific ESCALAB 250Xi spectrometer and all the binding energies were calibrated using the characteristic C 1s peak at 284.8 eV. The Brunauer-Emmett-Teller (BET) specific surface areas and pore size of the materials were measured on Micromeritics ASAP 2460 Surface Area and Porosimetry analyzer at 77 K. The Raman spectra were determined by Gamry Refence 3000+iRaman with a 532 nm laser. X-ray absorption near-edge structure (XANES) and extended X-ray absorption fine structure (EXAFS) spectra were acquired at the BL14W1 station of Shanghai Synchrotron Radiation Facility (SSRF), China. Inductive coupled plasma optical emission spectroscopy (ICP-OES) results were collected by an Agilent ICPOES730 system. The ultraviolet-visible (UV-Vis) adsorption spectra were obtained by a UV-1900 spectrophotometer. Online differential electrochemical mass spectrometry (DEMS) was carried out using a quadrupole mass spectrometer (QAS 100, PrismaPlus). ^{1}H nuclear magnetic resonance (NMR) spectra were examined by a Bruker Avance 500 MHz spectrometer.

Preparation of working electrode. 5 mg catalyst samples, 50 μL of Nafion solution (5 wt%), and 950 μL isopropanol were uniformly mixed by an ultrasonic cell disruptor for 30 min to form a homogeneous black ink. Finally, 200 μL of the catalyst black ink was slowly loaded onto carbon paper (CP) with an area of 1 cm^2 and naturally dried (catalyst/CP loading: 1 mg cm^{-2}).

Electrochemical measurements. The electrochemical NO_3RR performance was examined by using an electrochemical workstation (CHI 660E) with a typical three-electrode system, using CoSb IMCs/CP, Ag/AgCl electrode and Pt wire as the working, reference and counter electrodes, respectively, in 0.1 M KOH with 500 ppm NO_3^--N solution. The electrochemical NO_3RR tests were determined using an H-type cell and the anode and cathode were separated by Nafion 211 membrane. The Nafion 211 membrane underwent a pretreatment process, which involved incubation in 5 wt% H_2O_2 solution at 50 °C for 1 h, followed by treatment with 0.1 M H_2SO_4 at 50 ℃ for 1 h, and subsequently rinsed with deionized water for multiple times. All potentials were converted into a reversible hydrogen electrode (RHE) ($E_{RHE} = E_{Ag/AgCl} + 0.059 \times pH + 0.197$ V).

Determination of NO_3^--N concentration. The concentration of NO_3^--N was determined using a colorimetric method. In detail, 100 uL of electrolyte is extracted from the electrolytic cell and diluted to 10 mL, then 2 ml was removed and added to the centrifuge tube. Subsequently, 2.6 ml of 0.05 M H_2SO_4 was added to the above centrifuge tube. The mixed solution was kept for 30 min under mild conditions, and the UV-Vis absorption spectra were collected. The absorbance value (A) was calculated by using the formula: $A=A_{220nm}-2A_{275nm}$. For calibration, various NO_3^--N solutions with known concentrations were used for calibration ($y = 0.114x + 0.008$, $R^2 = 0.999$).

Determination of NH_4^+-N concentration. The produced NH_4^+-N was determined via the indophenol blue method[1]. In detail, 100 uL of electrolyte was removed from the cathode electrolytic cell and

diluted to 10 mL, then 2 ml was removed and added to the centrifuge tube. Next, 2 ml of chromogenic agent solution containing 1.0 M NaOH, $C_7H_6O_3Na$ and 5 wt% $C_6H_5Na_3O_7 \cdot 2H_2O$, 1 ml of oxidizing agent solution containing 0.05 M NaClO, and 0.2 mL of 1 wt% $Na_2[Fe(NO)(CN)_5] \cdot 2H_2O$, were added to the above centrifuge tube. The mixed solution was kept for 1 h under mild conditions, and the concentration of NH_4^+-N was calculated by the absorbance measured at λ=655 nm, using a standard curve (y = 0.501x + 0.028, R^2=0.999), measured with standard NH_4Cl solutions with known concentrations.

The NH_3 selectivity is calculated based on the following equation:

$$NH_3\ selectivity = \frac{c_{NH_3\text{-}N}}{\Delta c_{NO_3^-\text{-}N}} \times 100\%$$

where $\Delta c_{NO_3^-\text{-}N}$ is the concentration change of NO_3^--N before and after electrolysis in ppm, $c_{NH_3\text{-}N}$ is the produced concentration of NH_3-N in ppm.

The NH_3 yield rate is calculated by the following equation:

$$NH_3\ yield = \frac{c_{NH_3} \times V}{t \times A}$$

where c_{NH_3} is the produced NH_3 concentration in ppm, V is the volume of the cathode electrolyte solution in L, t is the reduction time in h, A is the area of the carbon paper in cm^2.

The NH_3 Faradaic efficiency (*FE*) is calculated using the following equation:

$$FE = \frac{8 \times F \times c_{NH_3} \times V}{17 \times Q} \times 100\%$$

where F is the Faradaic constant (96485 C mol^{-1}), c_{NH_3} is the produced NH_3 concentration in ppm, V is the volume of the cathode electrolyte solution in L, Q is the total electric charge in C.

Determination of NO_2^--N concentration. The produced NO_2^--N was determined by the Griess reagent. Firstly, the Griess reagent was prepared by mixing 0.1g of $C_{12}H_{14}N_{22} \cdot 2HCl$, 1.0 g of $C_6H_8N_2O_2S$, 2.94 mL of H_3PO_4 and 50 mL of H_2O. To determine the concentration of NO_2^--N, 1 mL

electrolyte was added to the centrifuge tube and mixed with 2.0 mL H_2O and 1.0 mL color reagent. The mixed solution was kept for 10 min at room temperature and the concentration of NO_2^--N was calculated by the absorbance measured at λ=540 nm, using a standard curve (y = 0.751x + 0.003, R^2=0.999), a series of $NaNO_2$ solution with known concentrations were used for calibration.

Determination of N_2H_4-N concentration. The produced N_2H_4-N was determined through the Watt and Chrisp method[2]. Firstly, a color reagent was prepared by mixing 3 g of p-$C_9H_{11}NO$, 15 mL of HCl and 150 mL of ethanol. To determine the concentration of N_2H_4-N, 5 mL of color reagent was added to 5 mL of the cathode electrolytic. The mixed solution was kept for 30 min under room temperature and the concentration of N_2H_4-N was calculated by the absorbance measured at λ=455 nm, using a standard curve (y = 0.315x + 0.036, R^2=0.999), various N_2H_4 solution with known concentrations were used for calibration.

Isotope labeling experiments. Isotope labeling experiments were conducted using $Na^{15}NO_3$ as the N source to investigate the source of NH_3. The electrolyte containing $^{15}NH_4^+$ was taken and the pH of the solution was adjusted to acidic by adding 0.1 M H_2SO_4. Subsequently, 50 μL of D_2O containing 4.4 mg/mL $C_4H_4O_4$ was added to the acidified solution (500 μL) for NMR testing. A calibration curve was generated using a standard $^{15}NH_4^+$ solution, featuring a positive linear agreement between the peak area ratio value and $^{15}NH_4^+$-^{15}N concentration.

Calculational methods and details. DFT calculations were performed with the Vienna ab initio simulation package (5.4.4 VASP) to explore the NO_3RR catalytic mechanism of CoSb (101) and Co (111)[3]. The Perdew-Burke-Enzzerhof (PBE) functional[4], projector augmented wave (PAW) method[5], and generalized gradient approximation (GGA) were used to optimize all structures and investigate the ions-electrons interactions for the whole NO_3RR process. Additionally, the van der Waals

interaction was corrected by the DFT-D3 method[6, 7]. All samples employed a cutoff energy of 500 eV and a 3×3×1 Monkhorst-Pack k-point mesh in the structure optimization process. The convergence criterions of 0.03 eV $Å^{-1}$ for force and 10^{-5} eV for total energy were chosen. And 15 Å vacuum layer was used along the z-direction to avoid vertical interactions between slabs. The reaction Gibbs free energy (ΔG) of each elementary reaction can be computed by the following equation:

$$\Delta G = \Delta E + \mathrm{ZPE} - T\Delta S$$

where ΔE denotes the electronic energy difference, ZPE is the zero-point energy, ΔS refers to the entropy (S) change between products and reactants, and T presents the reaction temperature (298.15 K).

The adsorption energy (E_A) of NO_3^- was calculated based on the following equation:

$$E_A = E_{*NO3} + E_{*} - E_{NO3}$$

where E_{*NO3} denotes the total energy of the adsorbed system, E_{*} is the energy of the slab, E_{NO3} refers to the energy of a single NO_3 group.

Zn-NO_3^- battery measurements. The Zn-NO_3^- battery test was determined in an H-cell divided by a Nafion 211 membrane. The anode compartment contains 1 M KOH as the electrolyte, whereas the cathode compartment employs 1 M KOH with 0.1 M $NaNO_3$. A polished zinc plate (1 cm^2) served as the anode, CoSb IMCs/C on carbon paper was used as the cathode.

Supplementary Figures

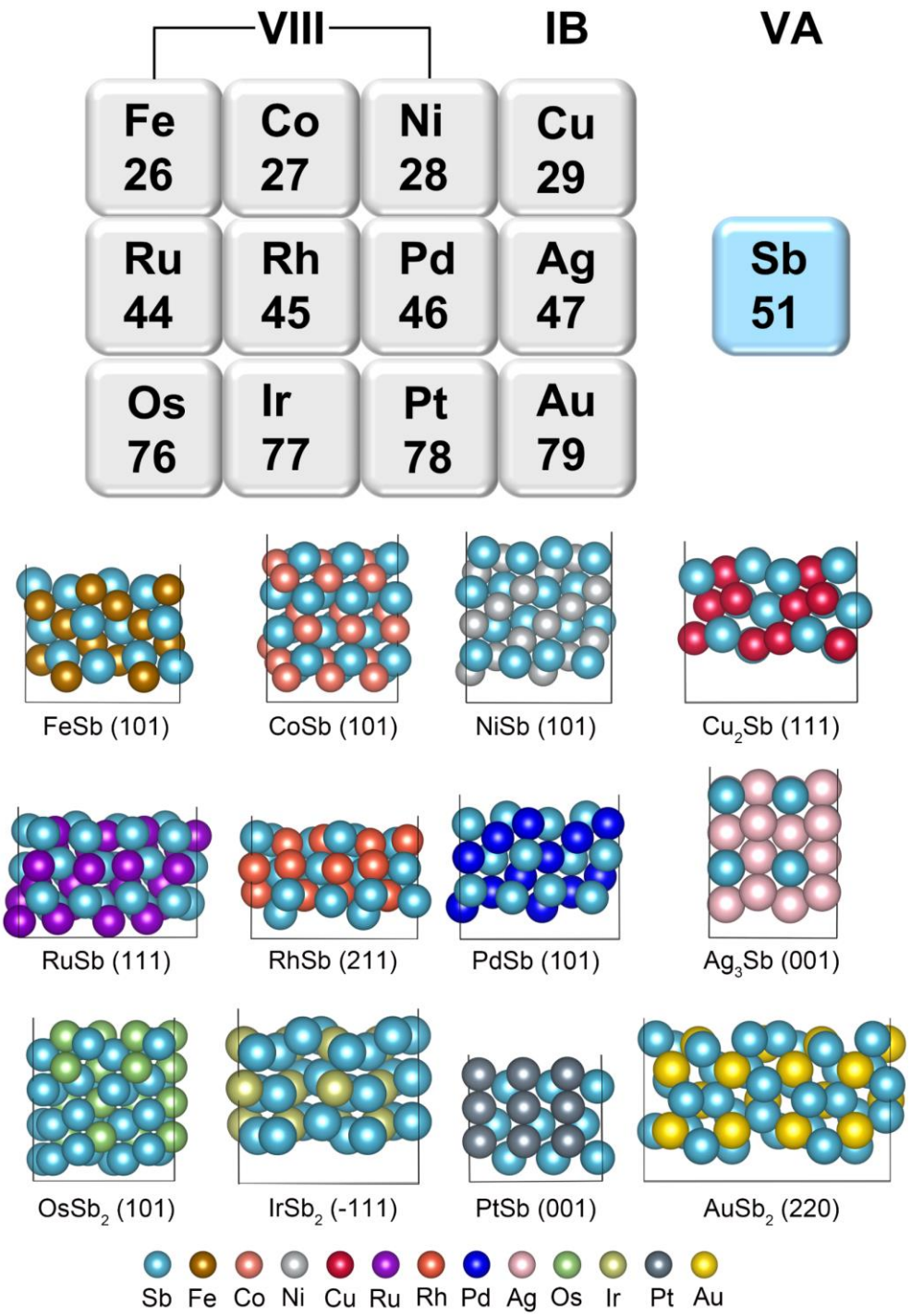

Supplementary Fig. 1 | Optimized structural models for Sb-based IMCs. Optimized structural models of hexagonal FeSb IMC, hexagonal CoSb IMC, hexagonal NiSb IMC, tetragonal Cu_2Sb IMC, orthorhombic RuSb IMC, orthorhombic RhSb IMC, hexagonal PdSb IMC, orthorhombic Ag_3Sb IMC, orthorhombic $OsSb_2$ IMC, monoclinic $IrSb_2$ IMC, hexagonal PtSb IMC, cubic $AuSb_2$ IMC.

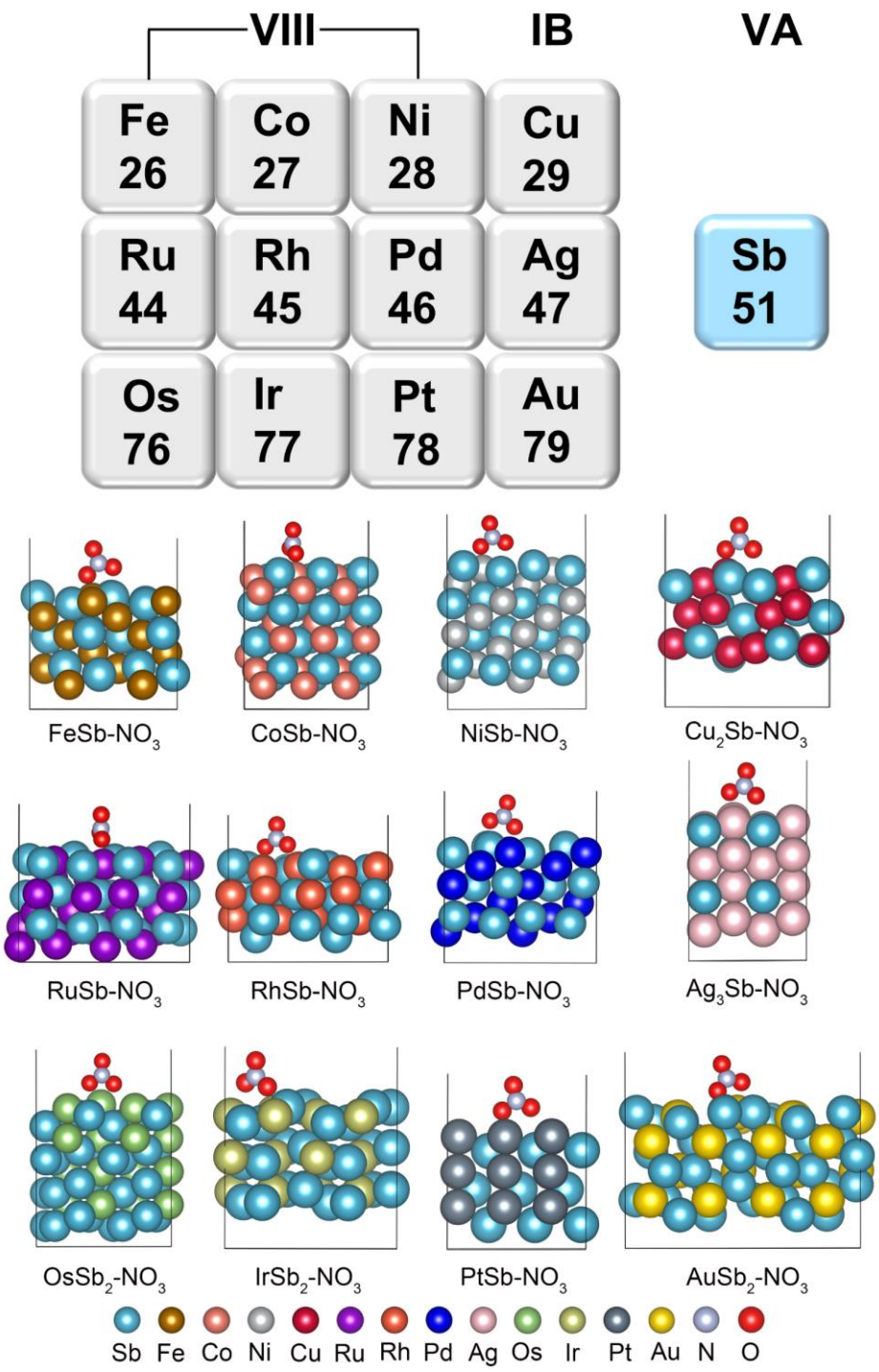

Supplementary Fig. 2 | Optimized structural models of *NO_3 intermediate on Sb-based IMCs.

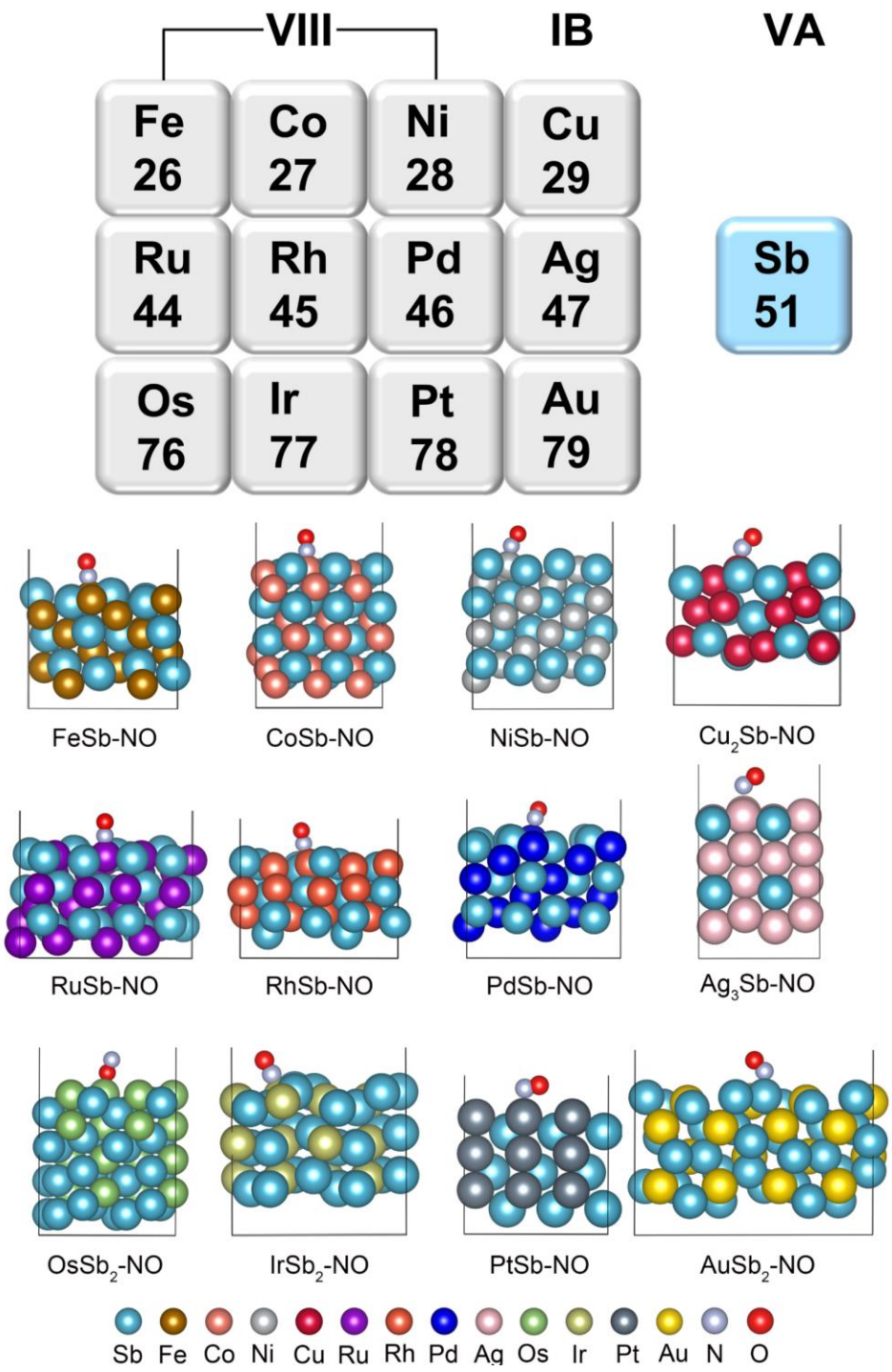

Supplementary Fig. 3 | Optimized structural models of *NO intermediate on Sb-based IMCs.

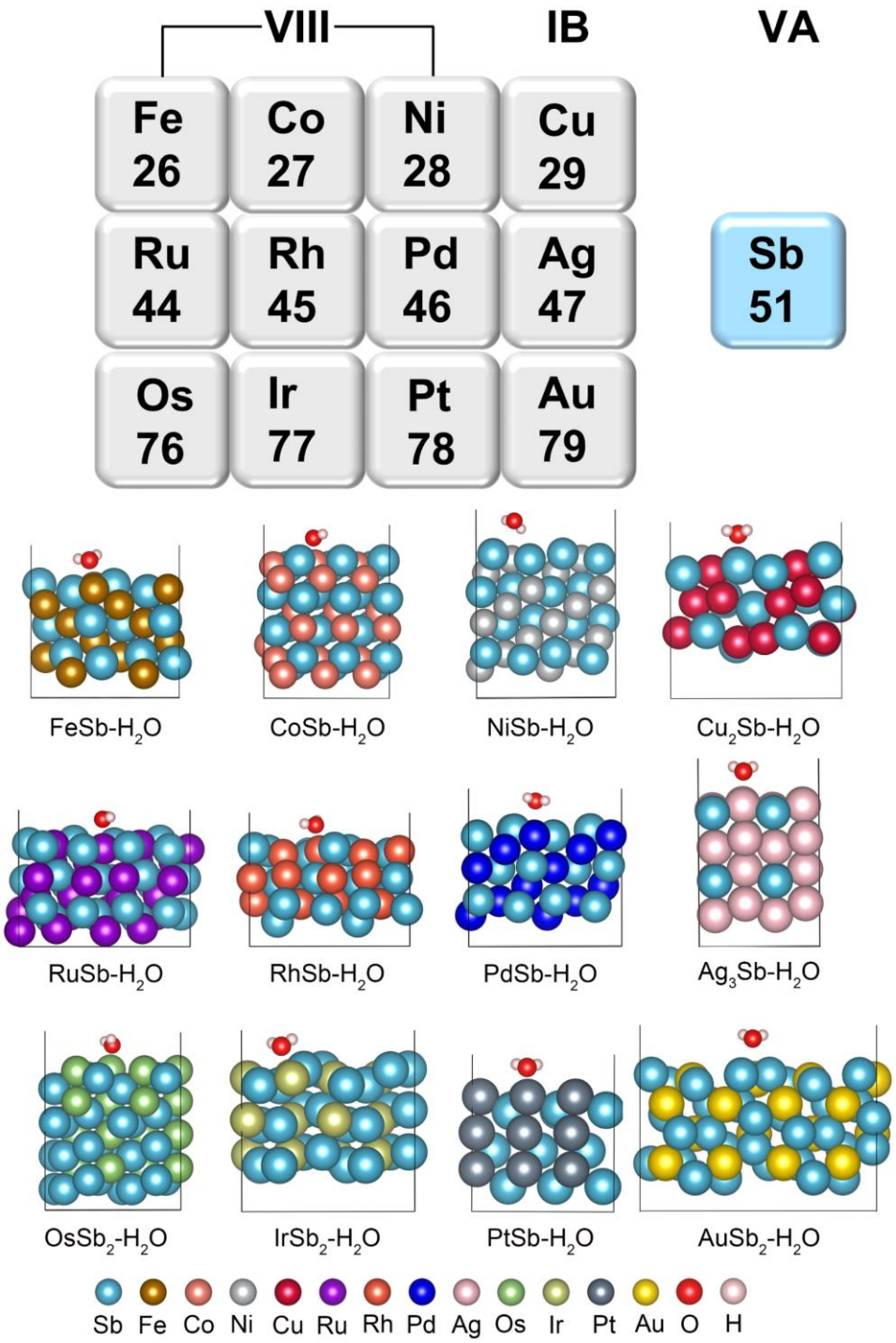

Supplementary Fig. 4 | Optimized structural models of *H_2O intermediate on Sb-based IMCs.

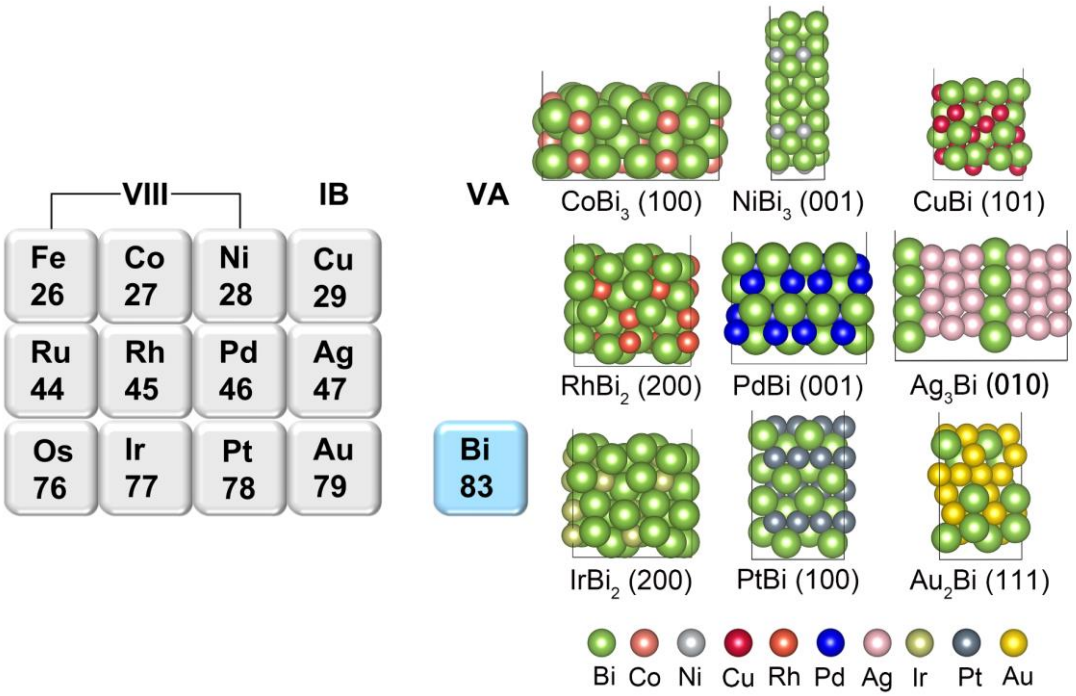

Supplementary Fig. 5 | Optimized structural models for Bi-based IMCs. Optimized structural models of orthorhombic $CoBi_3$ IMC, orthorhombic $NiBi_3$ IMC, hexagonal CuBi IMC, monoclinic $RhBi_2$ IMC, orthorhombic PdBi IMC, hexagonal Ag_3Bi IMC, monoclinic $IrBi_2$ IMC, hexagonal PtBi IMC and cubic Au_2Bi IMC. According to the phase diagram, there are no Fe-Bi, Ru-Bi and Os-Bi IMCs existing in the phase diagrams.

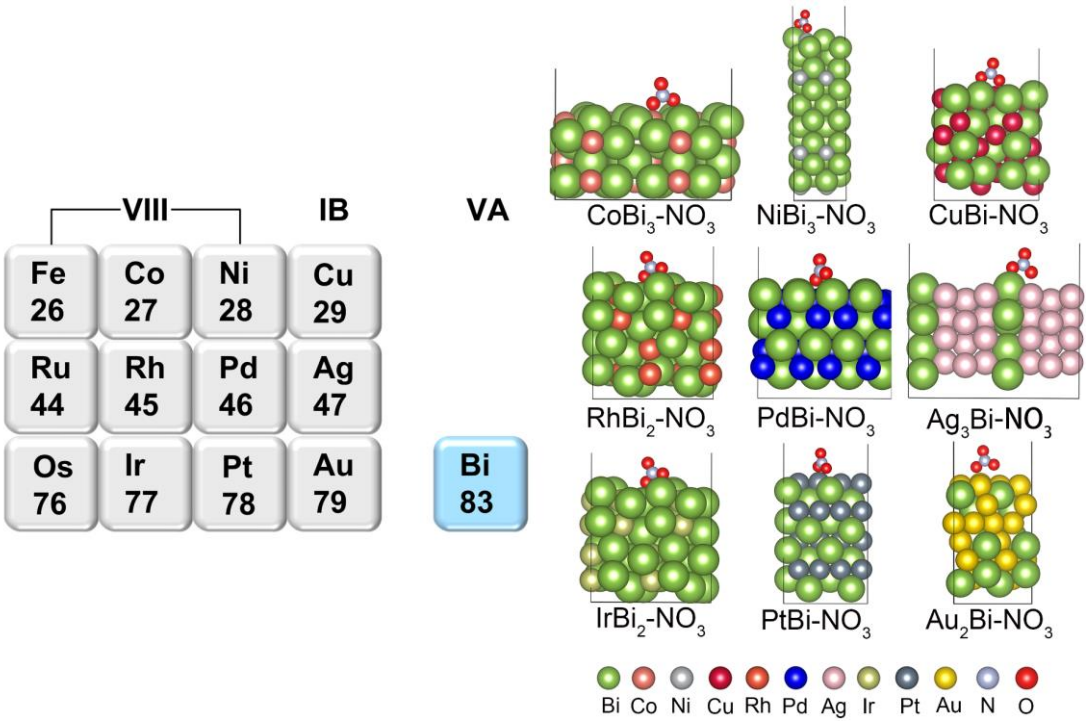

Supplementary Fig. 6 | Optimized structural models of *NO_3 intermediate on Bi-based IMCs.

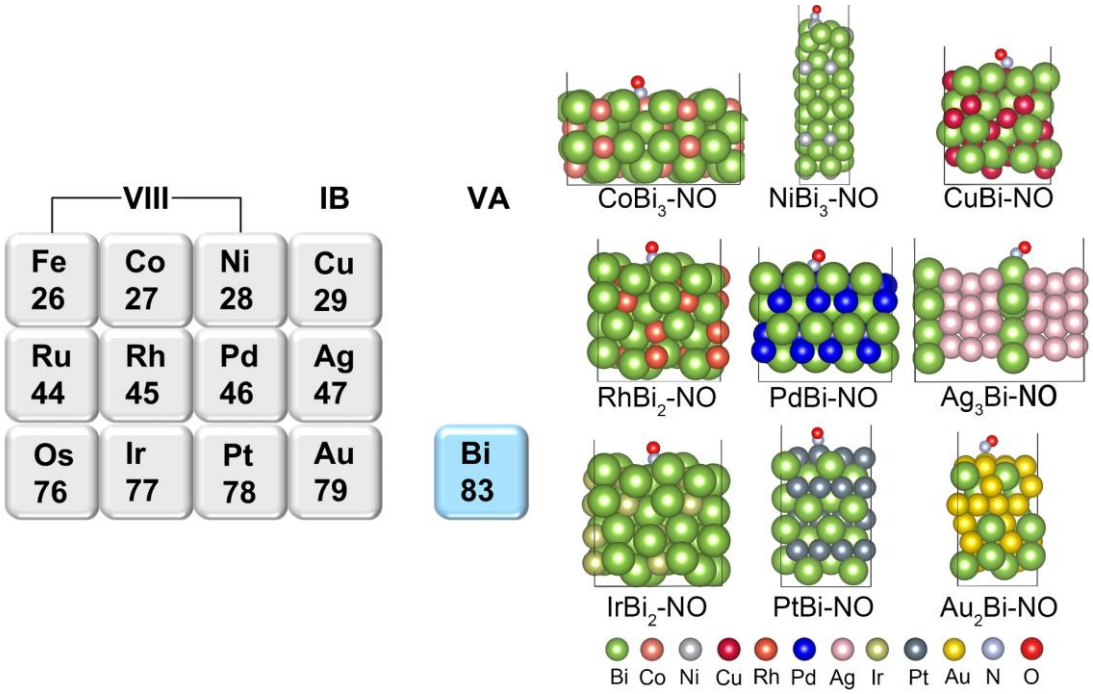

Supplementary Fig. 7 | Optimized structural models of *NO intermediate on Bi-based IMCs.

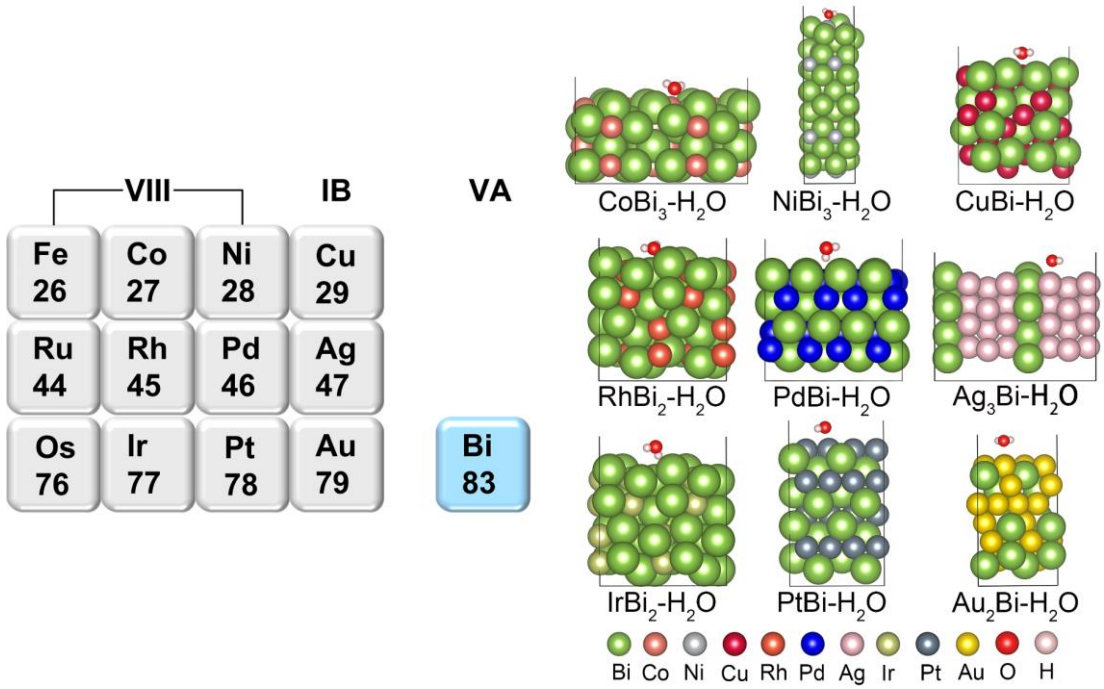

Supplementary Fig. 8 | Optimized structural models of *H_2O intermediate on Bi-based IMCs.

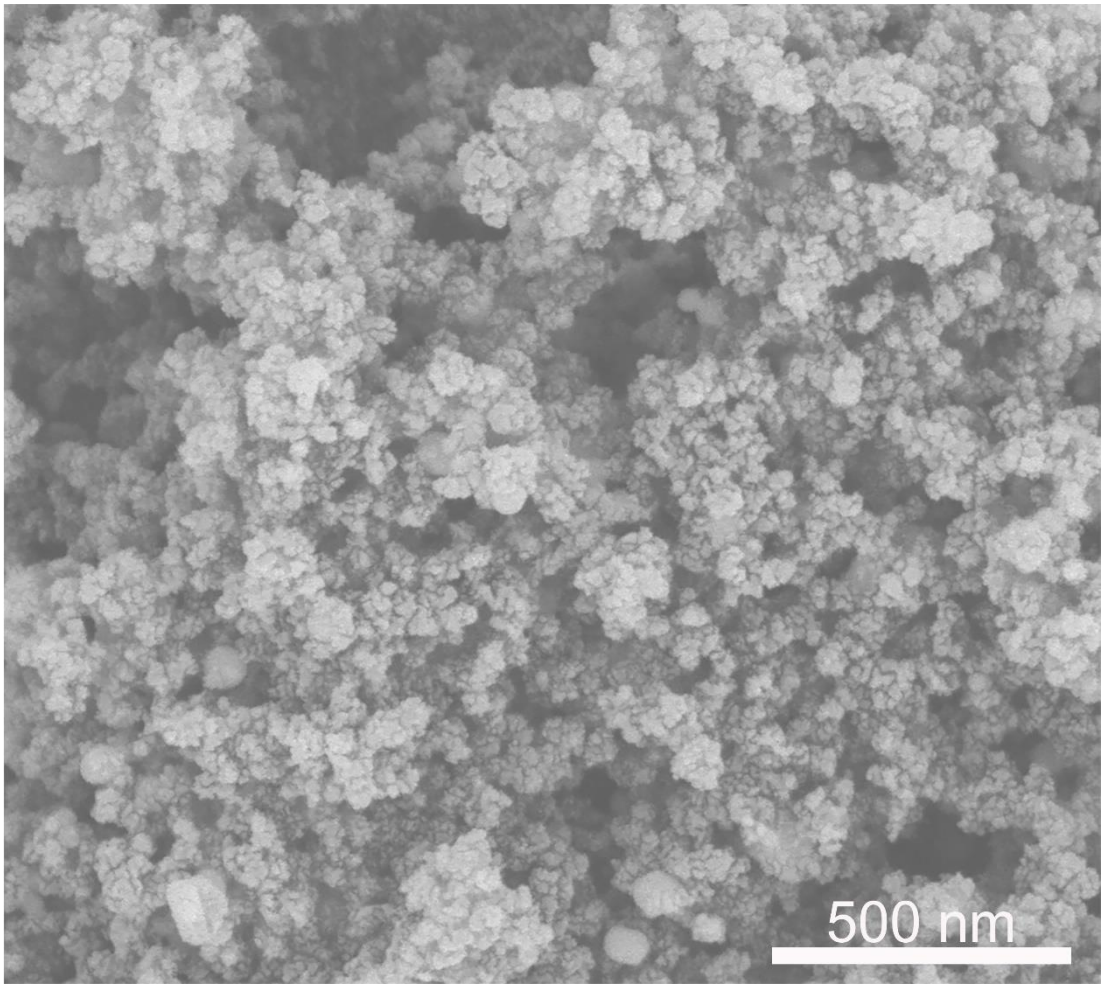

Supplementary Fig. 9 | SEM image of the as-prepared CoSb IMCs/C.

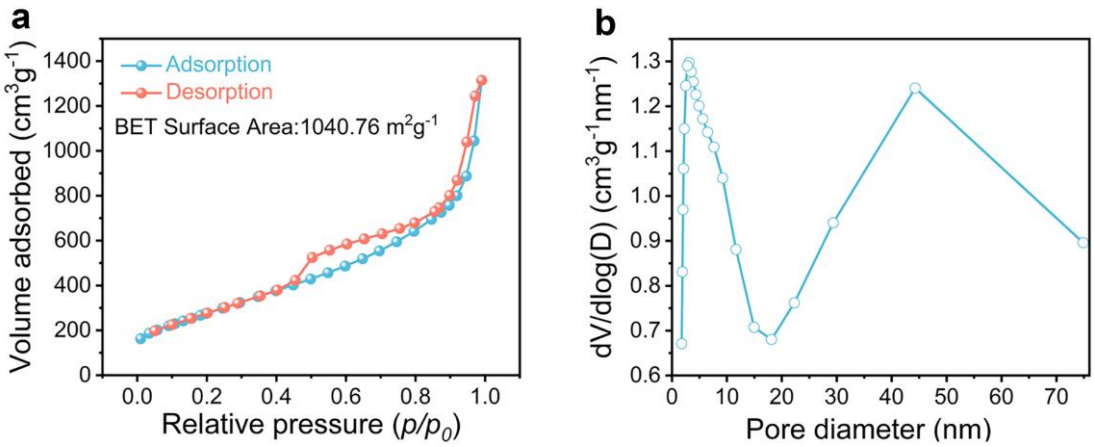

Supplementary Fig. 10 | BET analysis of CoSb IMCs/C. **a** N_2 adsorption-desorption isotherms. **b** The corresponding pore size distribution curve of CoSb IMCs/C.

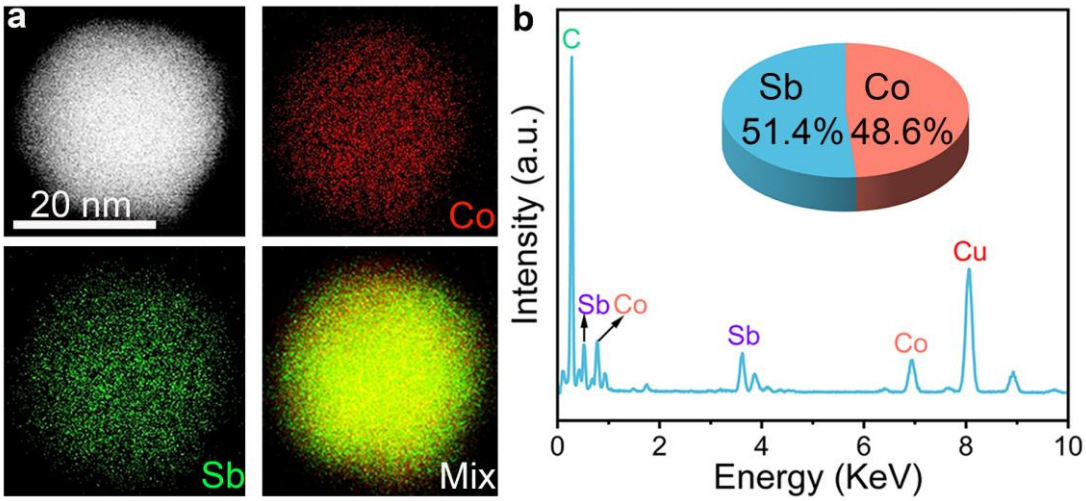

Supplementary Fig. 11 | EDX elemental mapping images and spectrum of CoSb IMCs/C. a HAADF-STEM image and the corresponding EDX elemental mapping images of an individual CoSb IMC. **b** EDX spectrum recorded from an individual CoSb IMC.

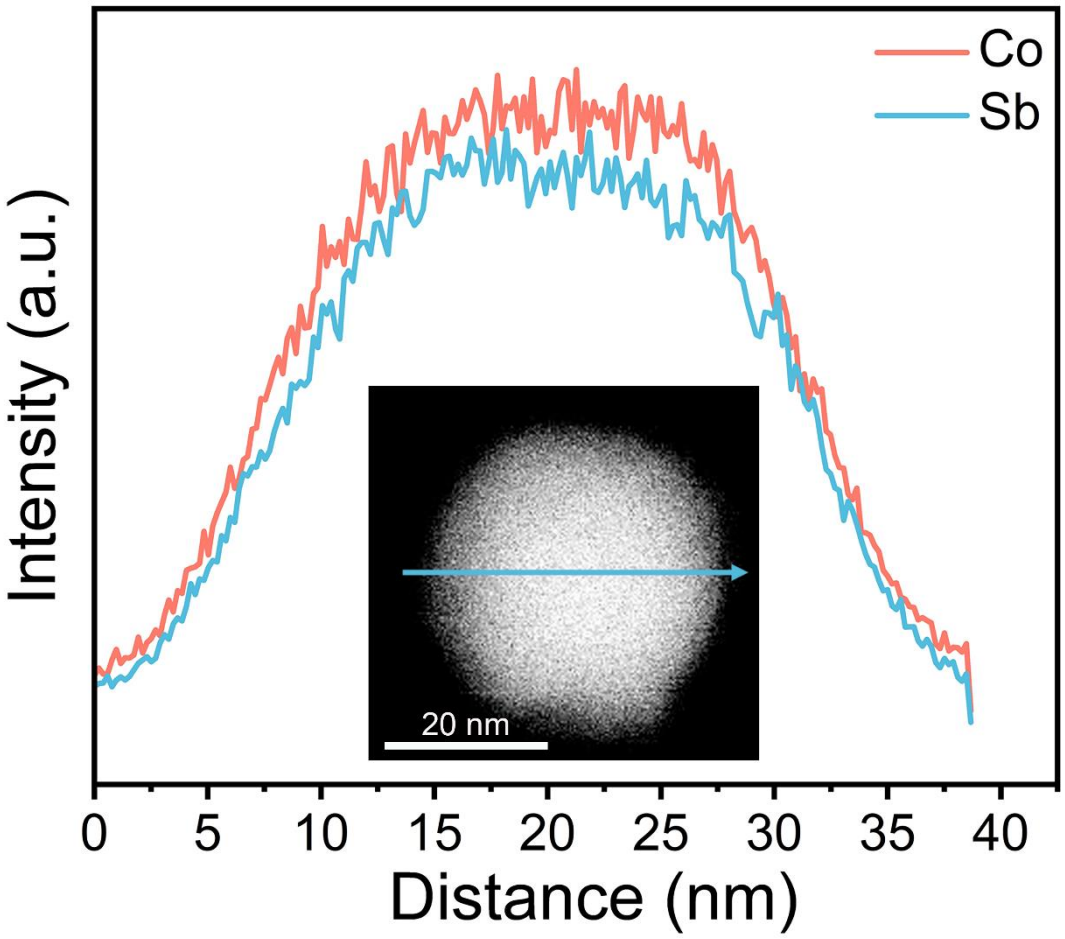

Supplementary Fig. 12 | EDX line scan profile recorded from an individual CoSb IMC.

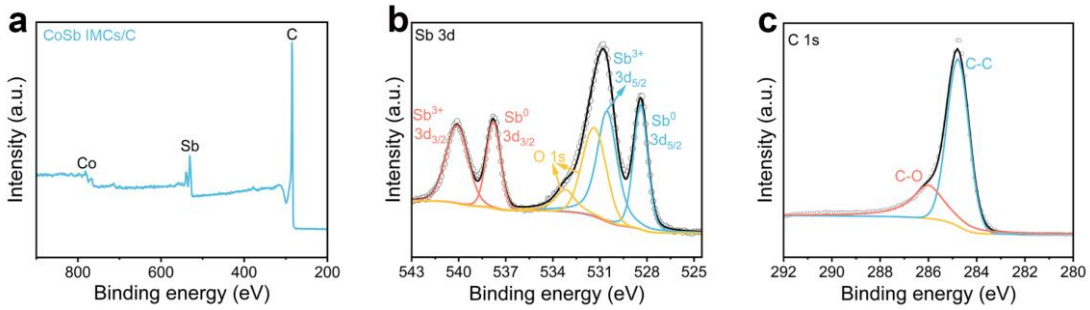

Supplementary Fig. 13 | XPS analyses of CoSb IMCs/C. a XPS survey spectrum. **b**, **c** High-resolution XPS spectra of Sb 3d (**b**), and C 1s (**c**) in CoSb IMCs/C.

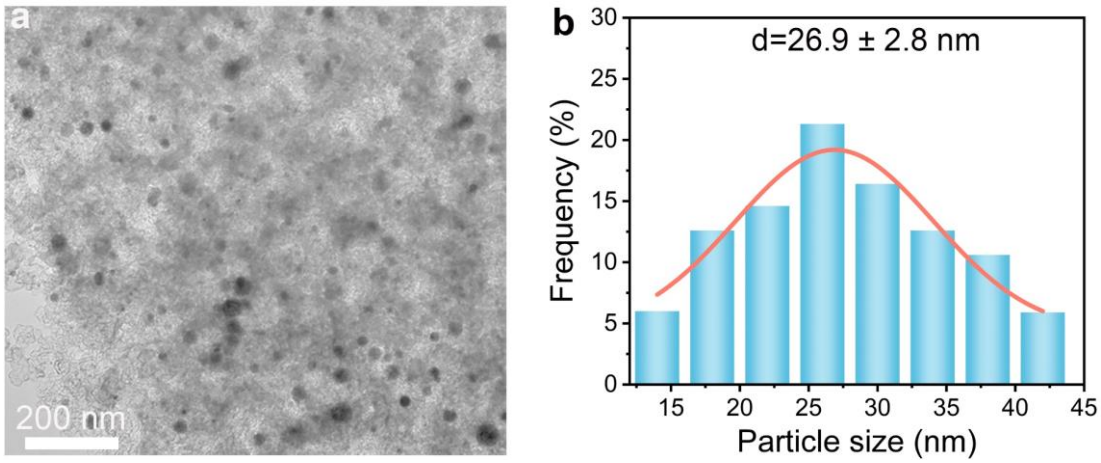

Supplementary Fig. 14 | TEM image and measured average particle size of Co NPs/C. a TEM image. **b** The corresponding particle size distribution histogram.

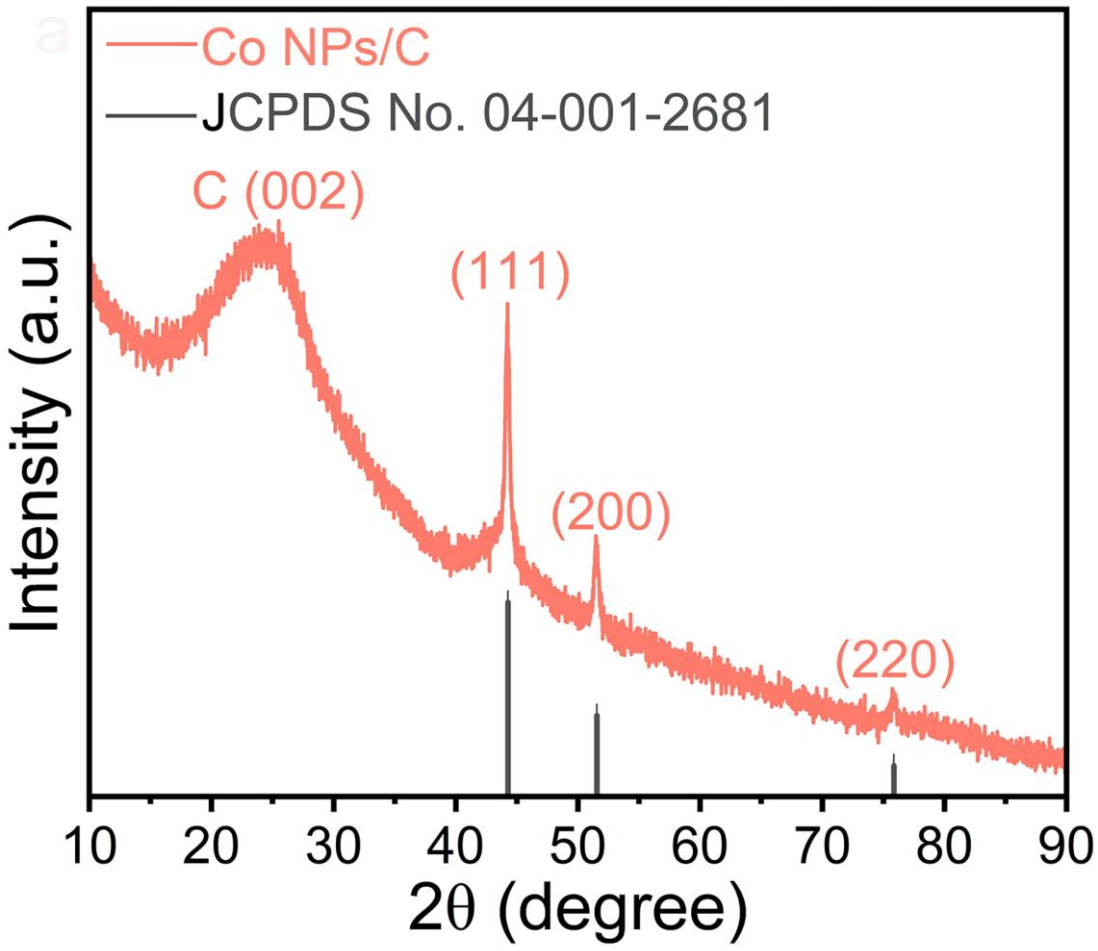

Supplementary Fig. 15 | XRD pattern of Co NPs/C.

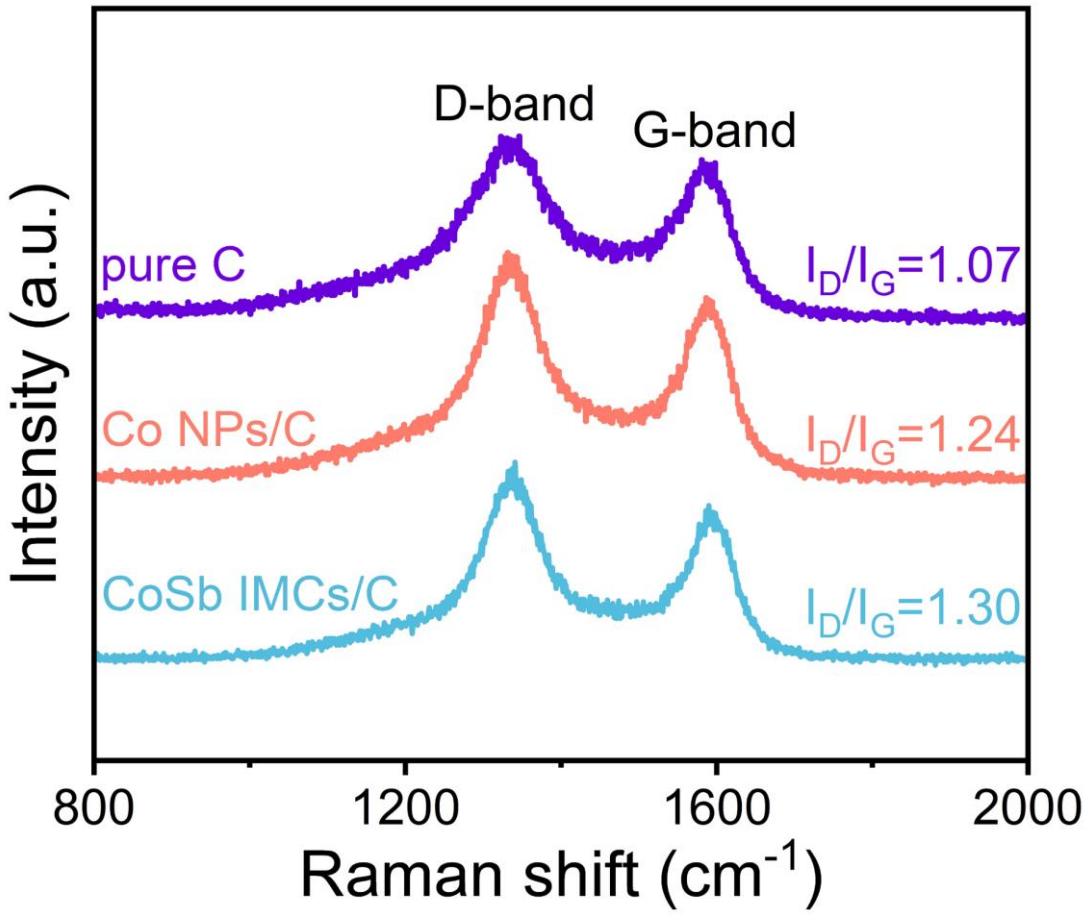

Supplementary Fig. 16 | Raman spectra of CoSb IMCs/C, Co NPs/C and pure carbon.

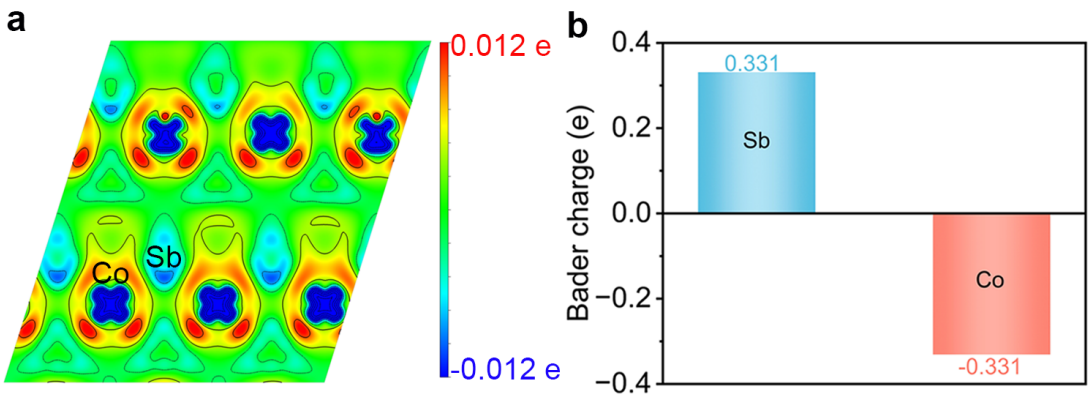

Supplementary Fig. 17 | The electronic distribution of CoSb IMCs. a, **b** The 2D charge density difference map (**a**) and the corresponding Bader charge (**b**) of CoSb (101).

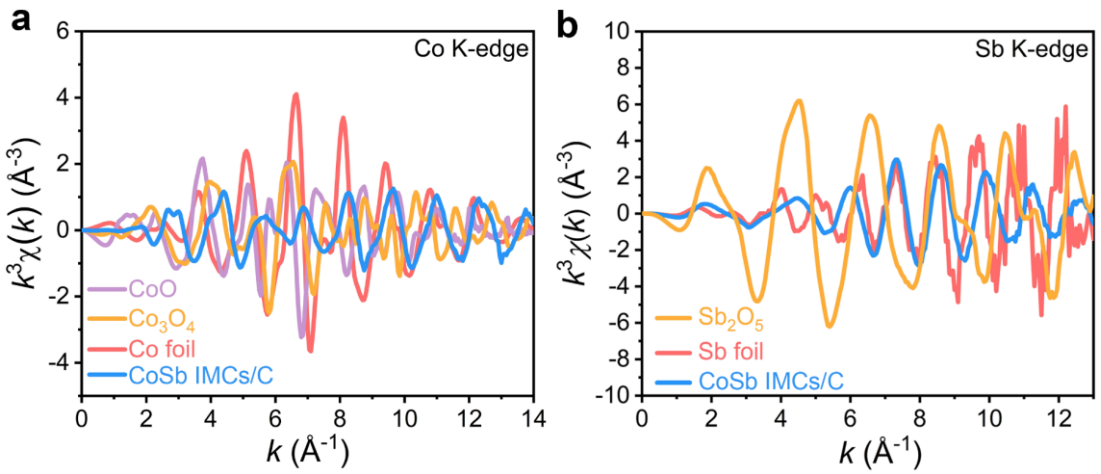

Supplementary Fig. 18 | Fourier-transformed EXAFS spectra. a Fourier-transformed EXAFS spectra at Co K-edge for CoO, Co_3O_4, Co foil and CoSb IMCs/C. **b** Fourier-transformed EXAFS spectra at Sb K-edge for Sb_2O_5, Sb foil and CoSb IMCs/C.

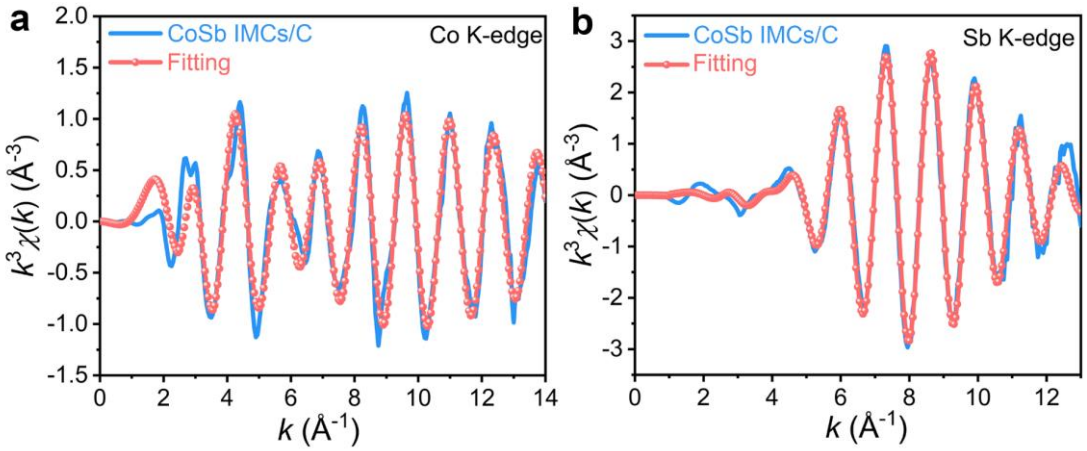

Supplementary Fig. 19 | EXAFS fitting curves. a, **b** EXAFS fitting curves at Co K-edge (**a**) and Sb K-edge (**b**) of CoSb IMCs/C in k-space.

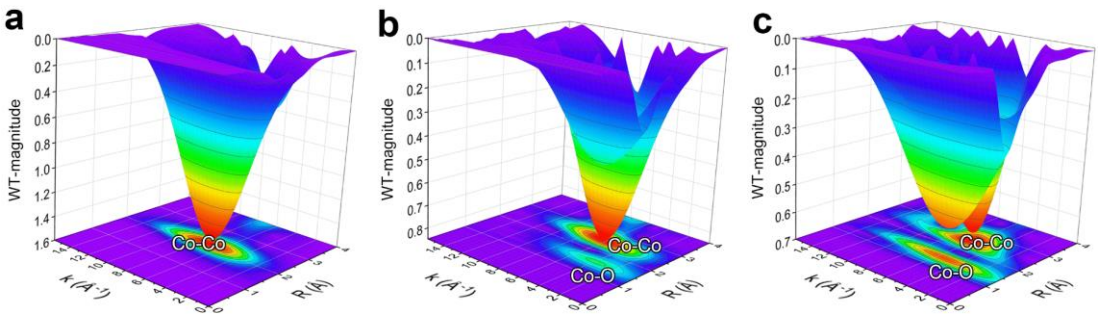

Supplementary Fig. 20 | WT -EXAFS spectra. a-c WT-EXAFS spectra at Co K-edge for Co foil (**a**), CoO (**b**) and Co_3O_4 (**c**).

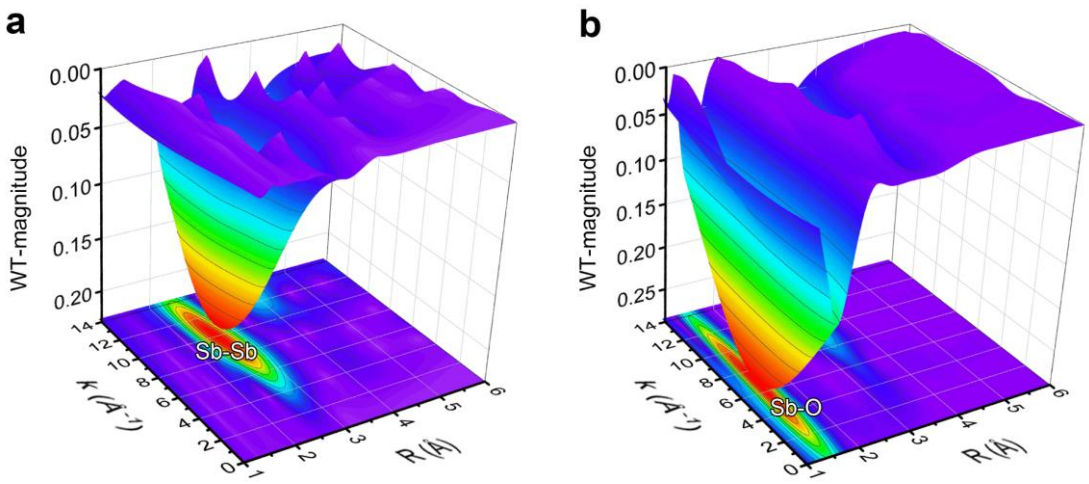

Supplementary Fig. 21 | WT-EXAFS spectra. a, **b** WT-EXAFS spectra at Sb K-edge of Sb foil (**a**) and Sb_2O_5 (**b**).

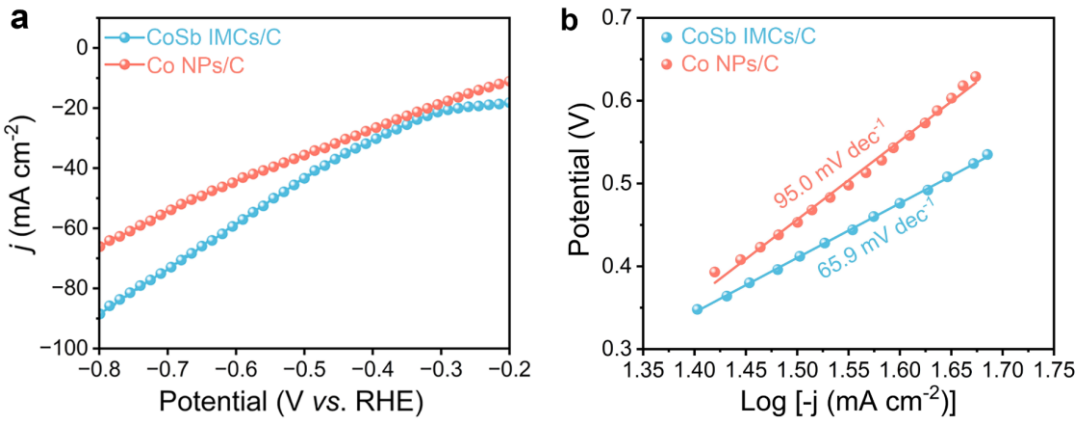

Supplementary Fig. 22 | Linear sweep voltammetry (LSV) curves and Tafel plots of Co NPs/C and CoSb IMCs/C. a LSV curves of Co NPs/C and CoSb IMCs/C in 0.1 M KOH with 500 ppm NO_3^--N. **b** The corresponding Tafel plots.

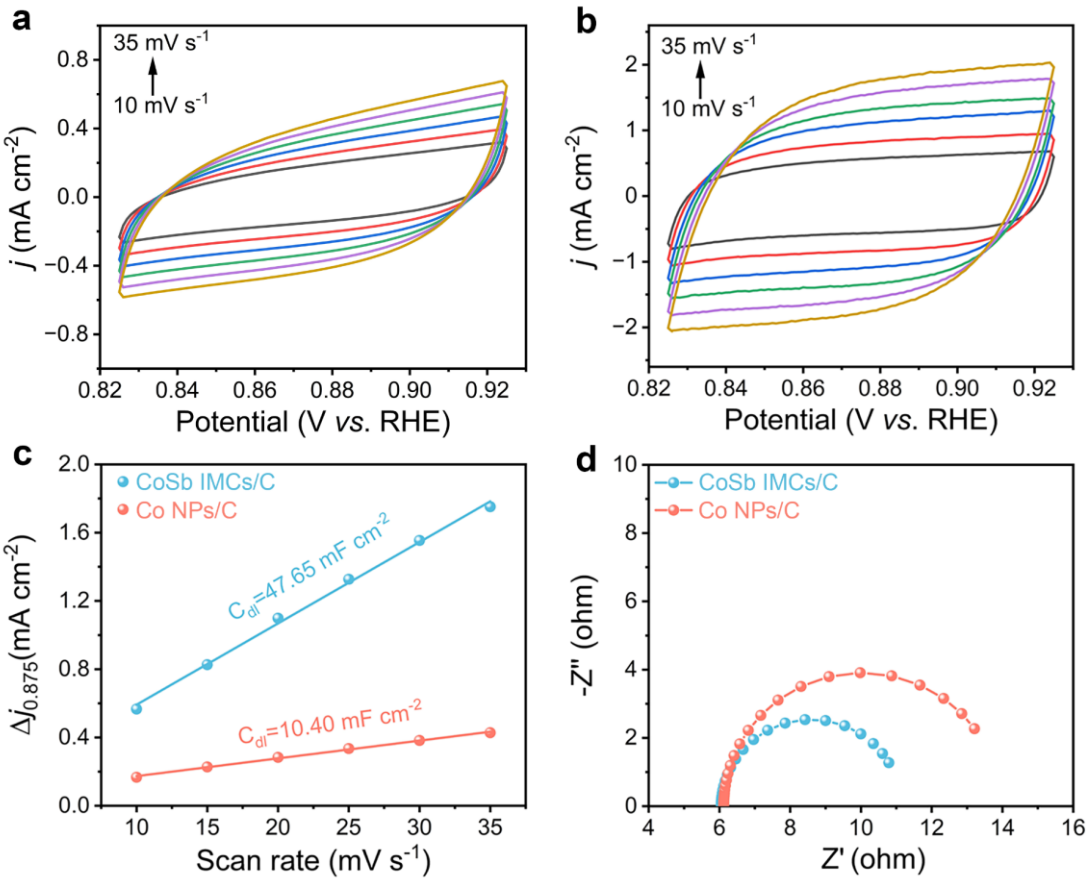

Supplementary Fig. 23 | Electrochemically active surface areas (ECSAs) and electrochemical impedance spectroscopy (EIS) curves of CoSb IMCs/C and Co NPs/C. a, **b** Cyclic voltammetry curves of Co NPs/C (**a**) and CoSb IMCs/C (**b**) with scan rates from 10 to 35 mV s^{-1} in 0.1 M KOH solution. **c** Calculated C_{dl} values of CoSb IMCs/C and Co NPs/C. **d** Nyquist plots of CoSb IMCs/C and Co NPs/C.

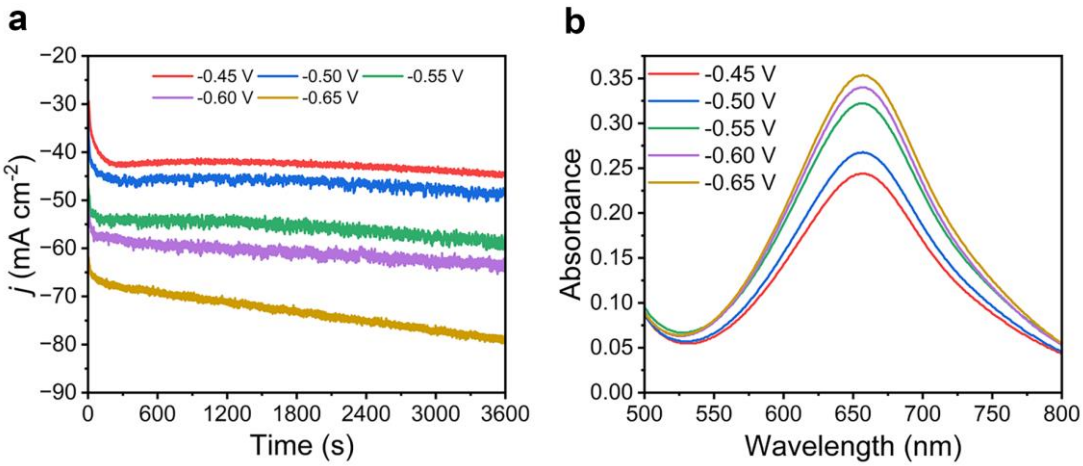

Supplementary Fig. 24 | Chronoamperometric (*j*-t) curves and UV-Vis spectra for quantification of NH_3 concentration. a, b The *j*-t curves (**a**) and UV-Vis absorption spectra (**b)** of CoSb IMCs/C at various potentials.

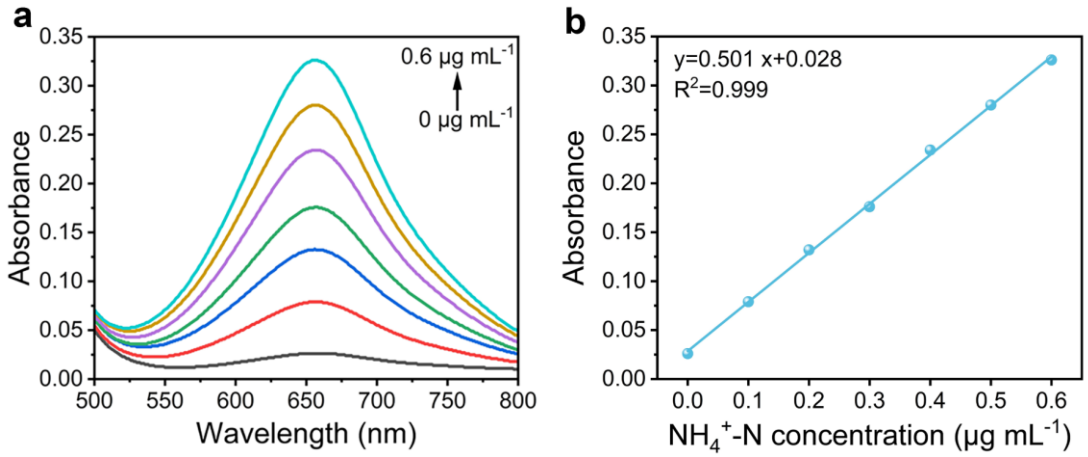

Supplementary Fig. 25 | The UV-Vis calibration curves of NH_4^+-N with different concentrations of NH_4Cl solutions as standards. a UV-Vis absorption spectra of NH_4^+-N solution with a series of concentrations in 0.1 M KOH solution. **b** Calibration curve used for calculation of NH_4^+-N concentrations.

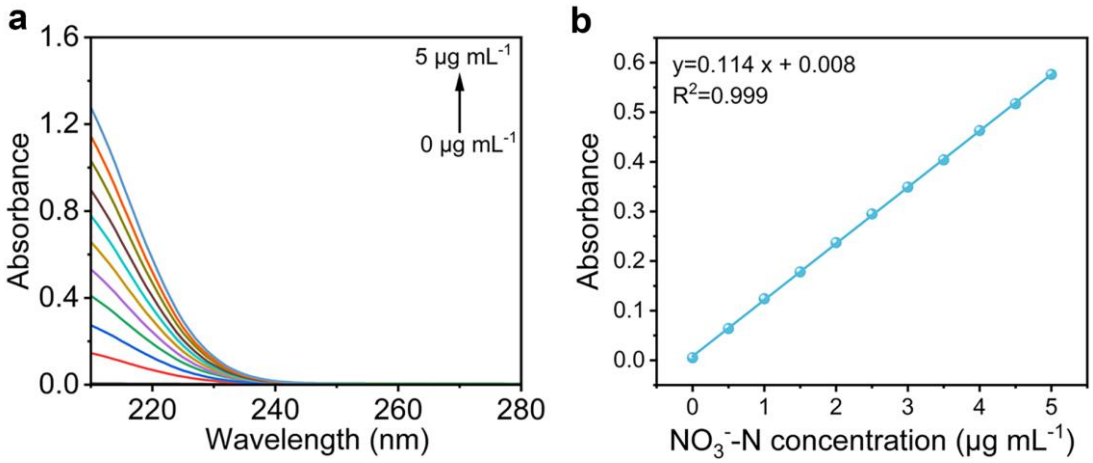

Supplementary Fig. 26 | The UV-vis calibration curves of NO_3^--N by using different concentrations of $NaNO_3$ solutions as standards. a UV-Vis absorption spectra of acidified NO_3^--N solution with various concentrations. **b** Calibration curve used for calculation of NO_3^--N concentrations.

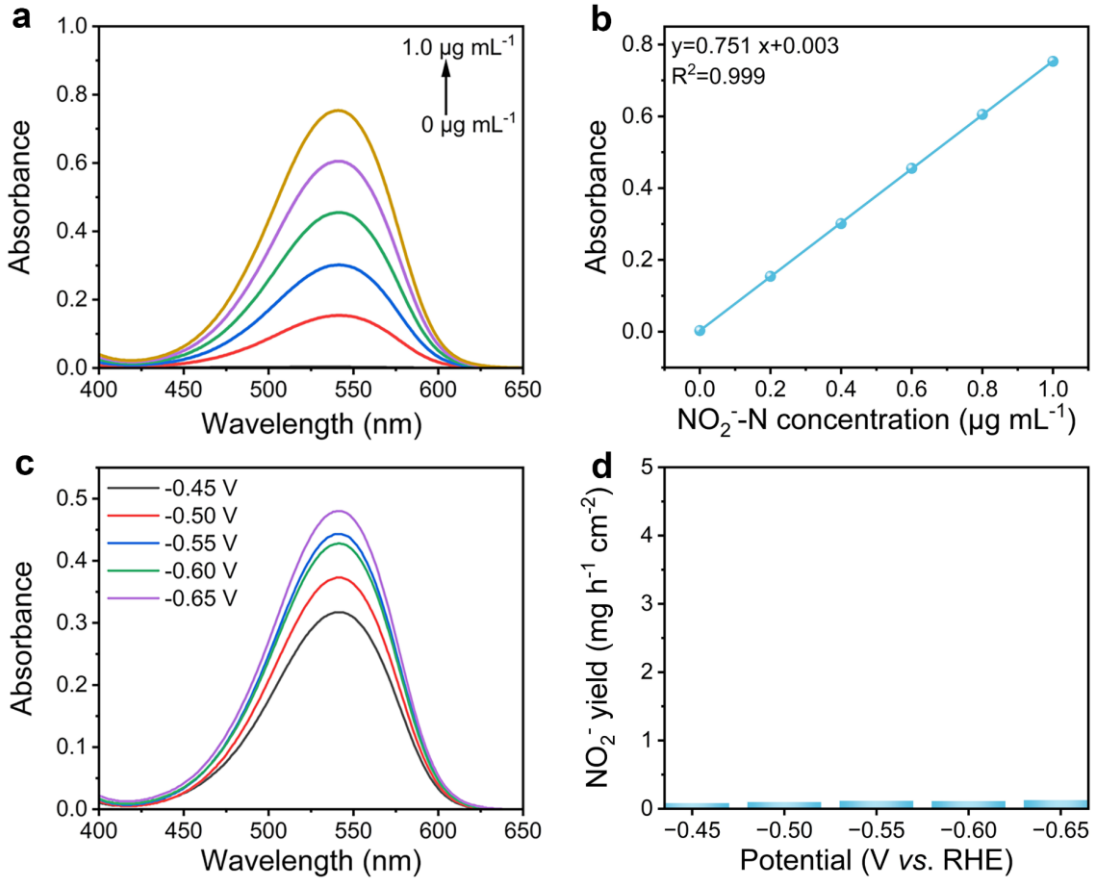

Supplementary Fig. 27 | The UV-vis calibration curves of NO_2^--N by using different concentrations of $NaNO_2$ solutions as standards and quantification of NO_2^- yield. a UV-Vis absorption spectra of NO_2^--N solution with different concentrations. **b** Calibration curve used for calculation of NO_2^--N concentrations. **c**, **d** UV-Vis absorption spectra (**c**) and the corresponding NO_2^- yield rates (**d**) at various potentials catalyzed by CoSb IMCs/C.

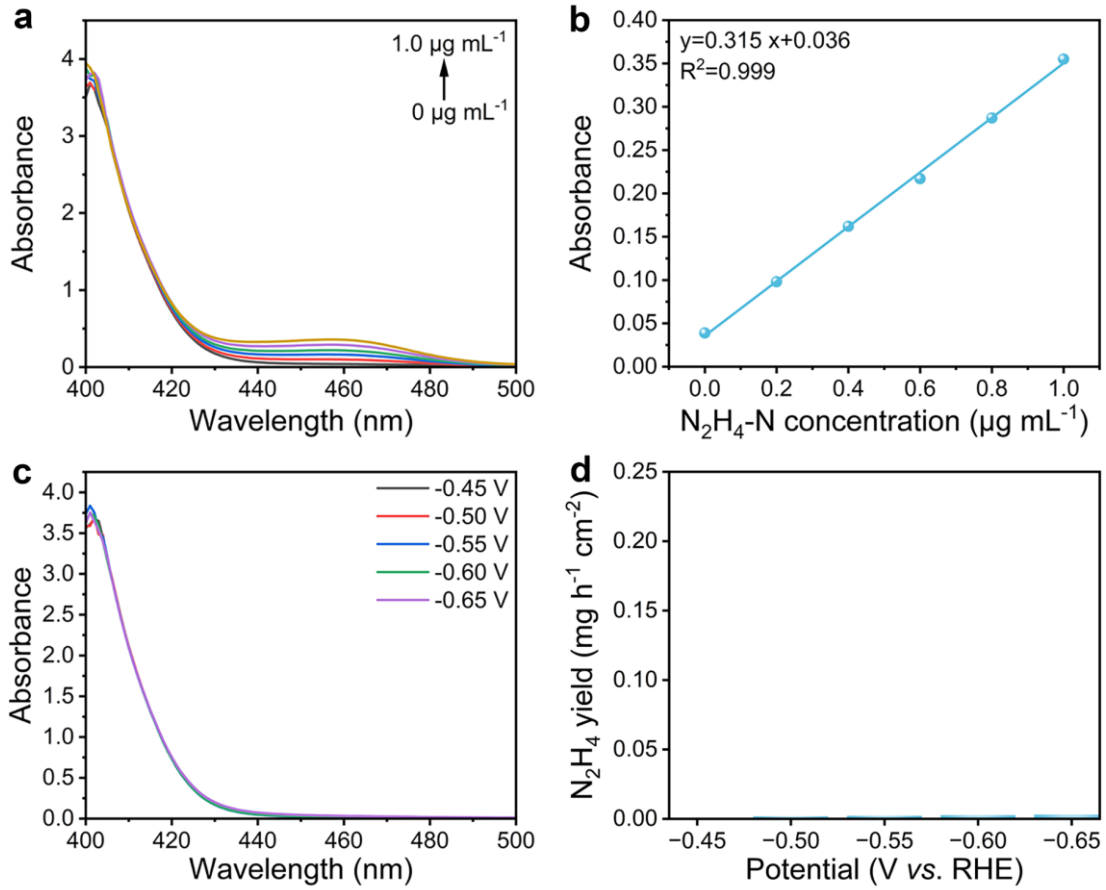

Supplementary Fig. 28 | The UV-vis calibration curves of N_2H_4-N by using different concentrations of N_2H_4 solutions as standards and quantification of N_2H_4 yield. a UV-Vis absorption spectra of N_2H_4-N solution with different concentrations. **b** Calibration curve used for calculation of N_2H_4-N concentrations. **c**, **d** UV-Vis absorption spectra (**c**) and the corresponding N_2H_4 yield rates (**d**) at various potentials catalyzed by CoSb IMCs/C.

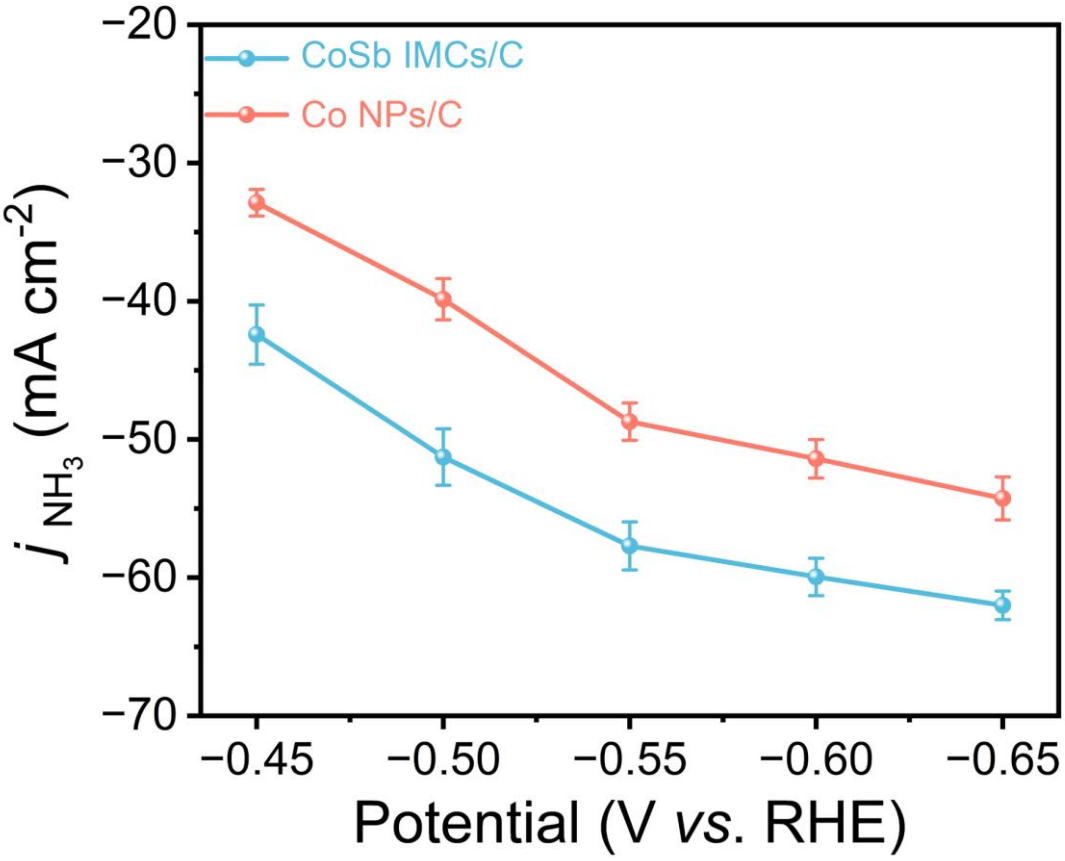

Supplementary Fig. 29 | Comparison of the NH_3 partial current density over CoSb IMCs/C and Co NPs/C at -0.55 V.

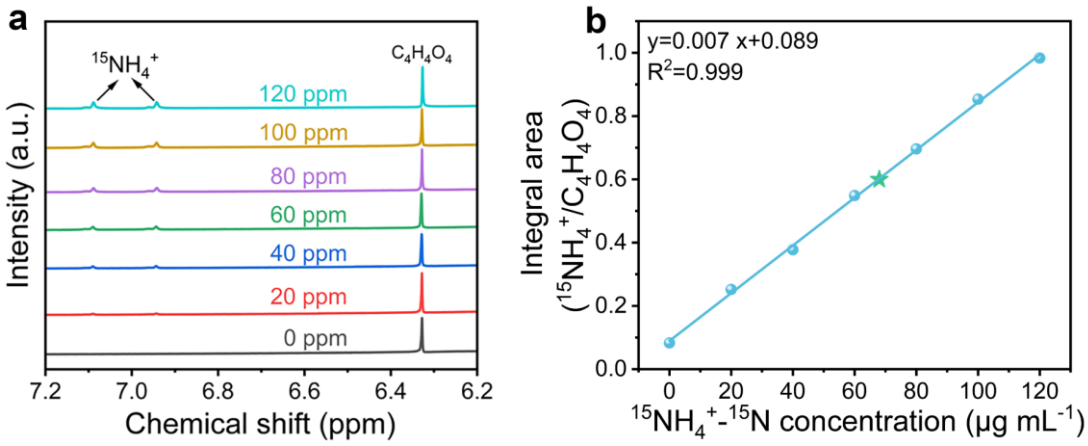

Supplementary Fig. 30 | The ^{1}H NMR calibration curves of $^{15}NH_4^+$ using different concentrations of $^{15}NH_4Cl$ solutions with $C_4H_4O_4$ as standards. a ^{1}H NMR spectra of standard $^{15}NH_4^+$ solutions with different concentrations. **b** The standard curve is used for the determination of $^{15}NH_4^+$-^{15}N concentration.

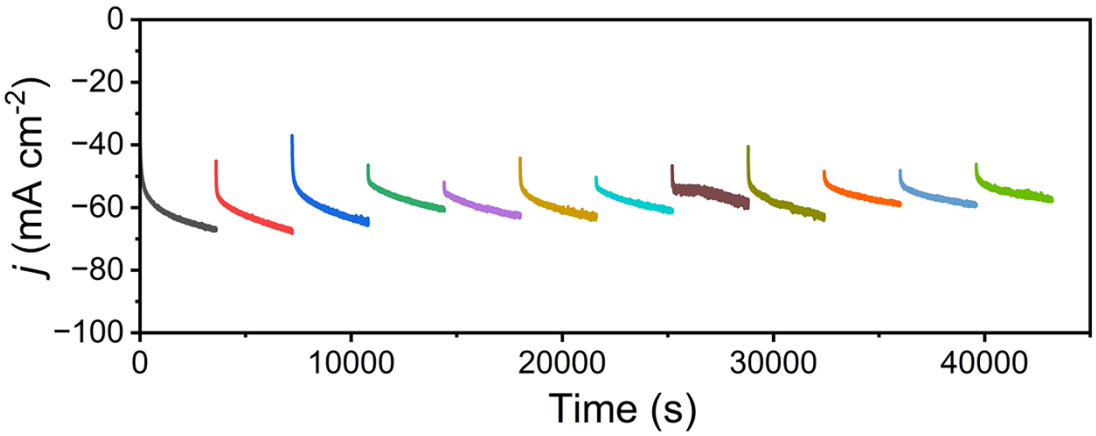

Supplementary Fig. 31 | Time-dependent current density curves for 12 consecutive cycles over CoSb IMCs/C for NO_3RR at -0.55 V.

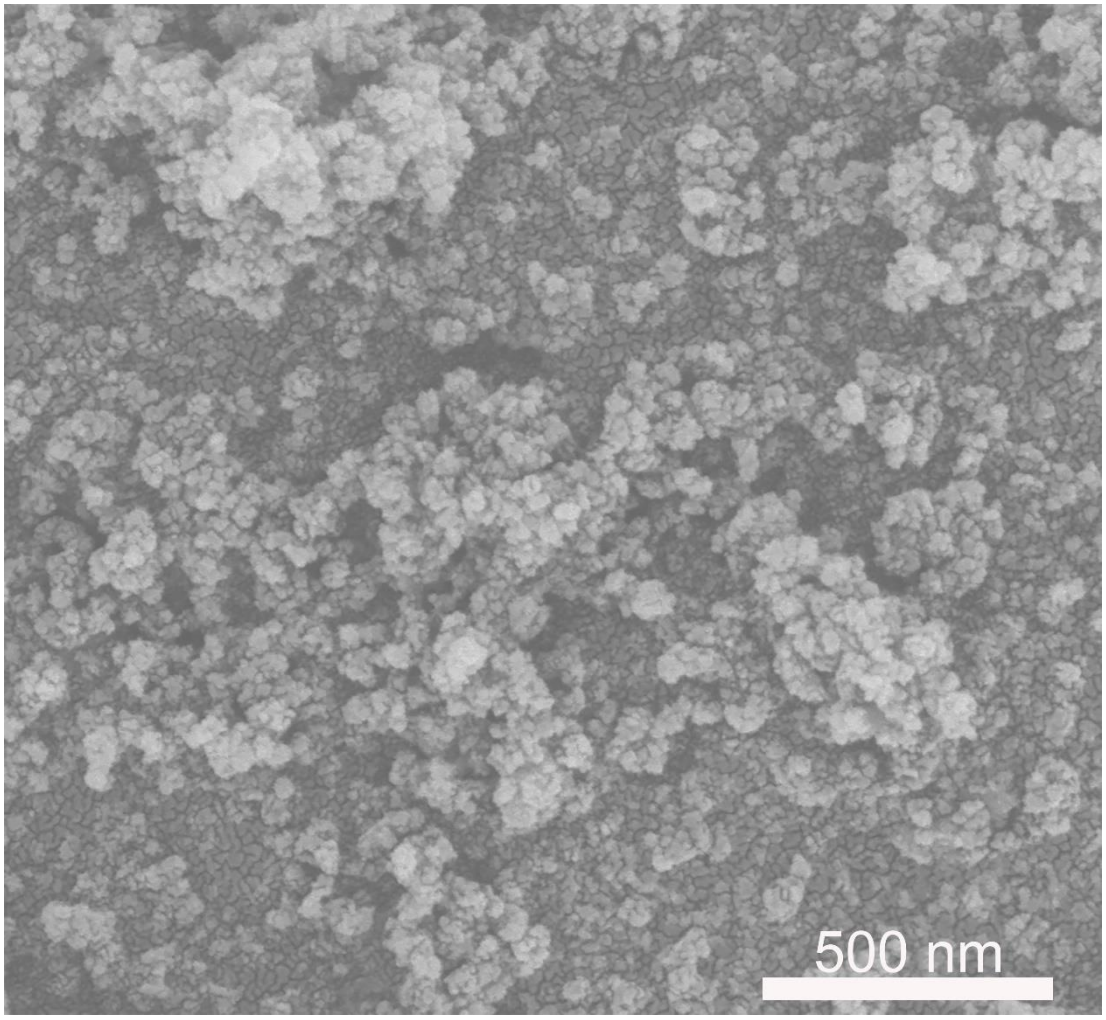

Supplementary Fig. 32 | SEM image of CoSb IMCs/C after the NO_3RR stability tests in 0.1 M KOH.

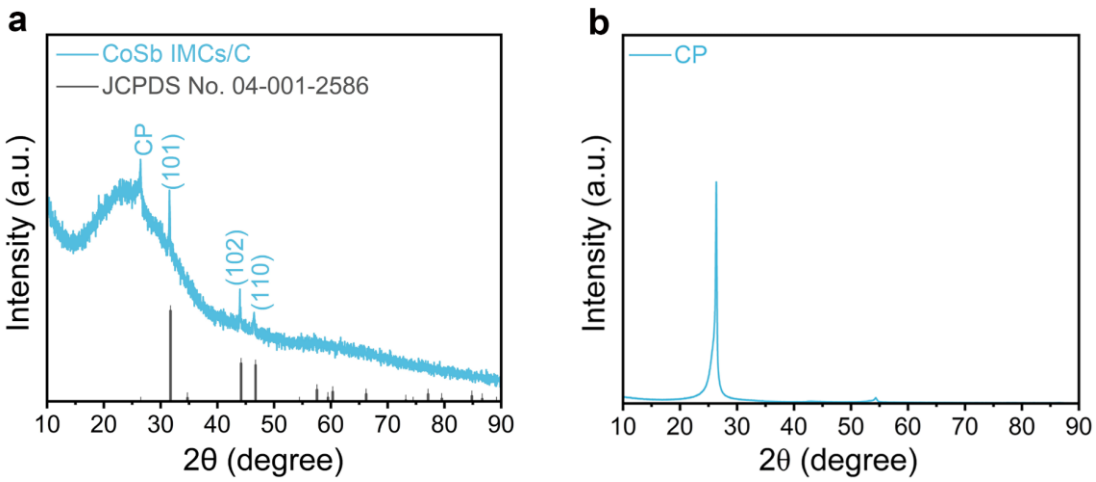

Supplementary Fig. 33 | XRD patterns. a, **b** XRD pattern of CoSb IMCs/C after the stability tests (**a**) and pure CP (**b**).

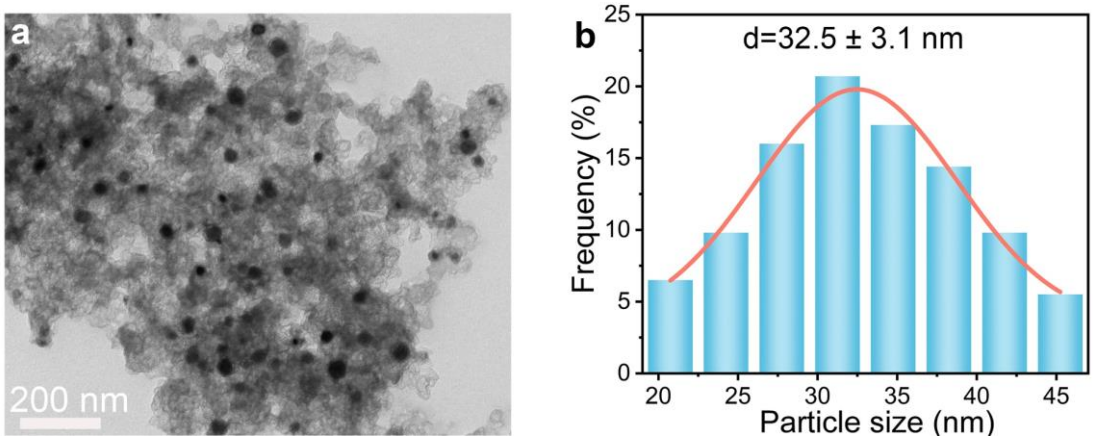

Supplementary Fig. 34 | Morphology characterizations of CoSb IMCs/C after the long-term stability tests. a TEM image of CoSb IMCs/C after the NO_3RR stability tests in 0.1 M KOH. **b** The corresponding particle size distribution histogram.

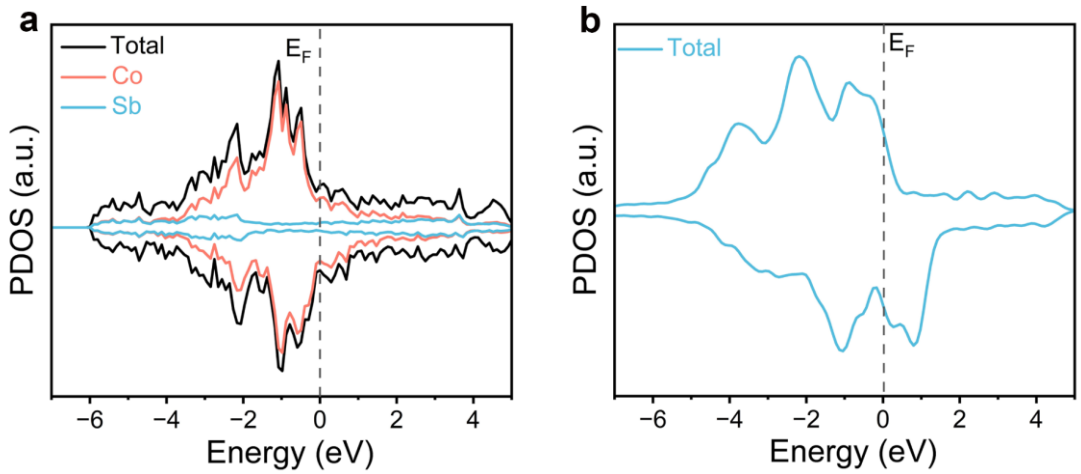

Supplementary Fig. 35 | Electronic structures. a, **b** The PDOS plots of CoSb (101) (**a**) and Co (111) (**b**).

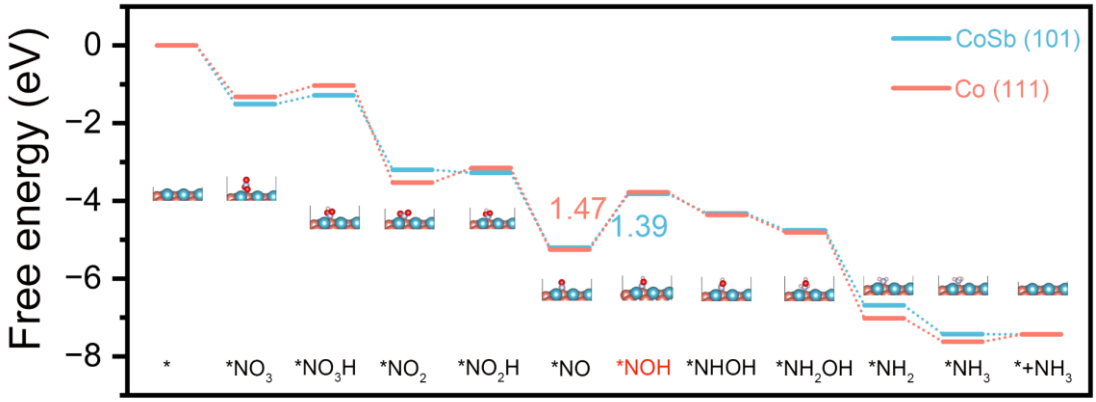

Supplementary Fig. 36 | Gibbs free energy diagrams for electrocatalytic NO_3RR pathways on Co (111) and CoSb (101) surfaces.

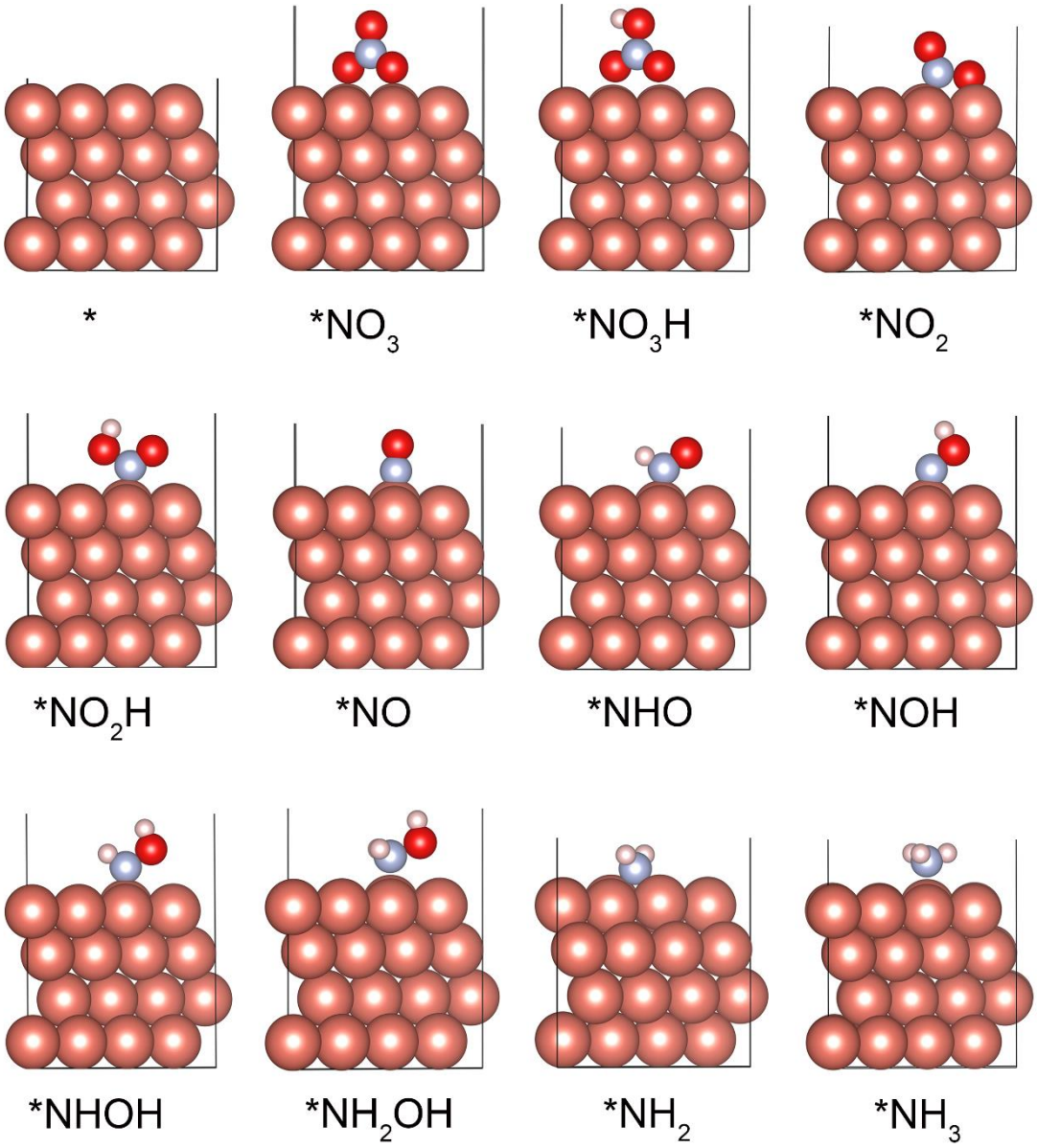

Supplementary Fig. 37 | Optimized structural models of reaction intermediates for NO_3RR on Co (111).

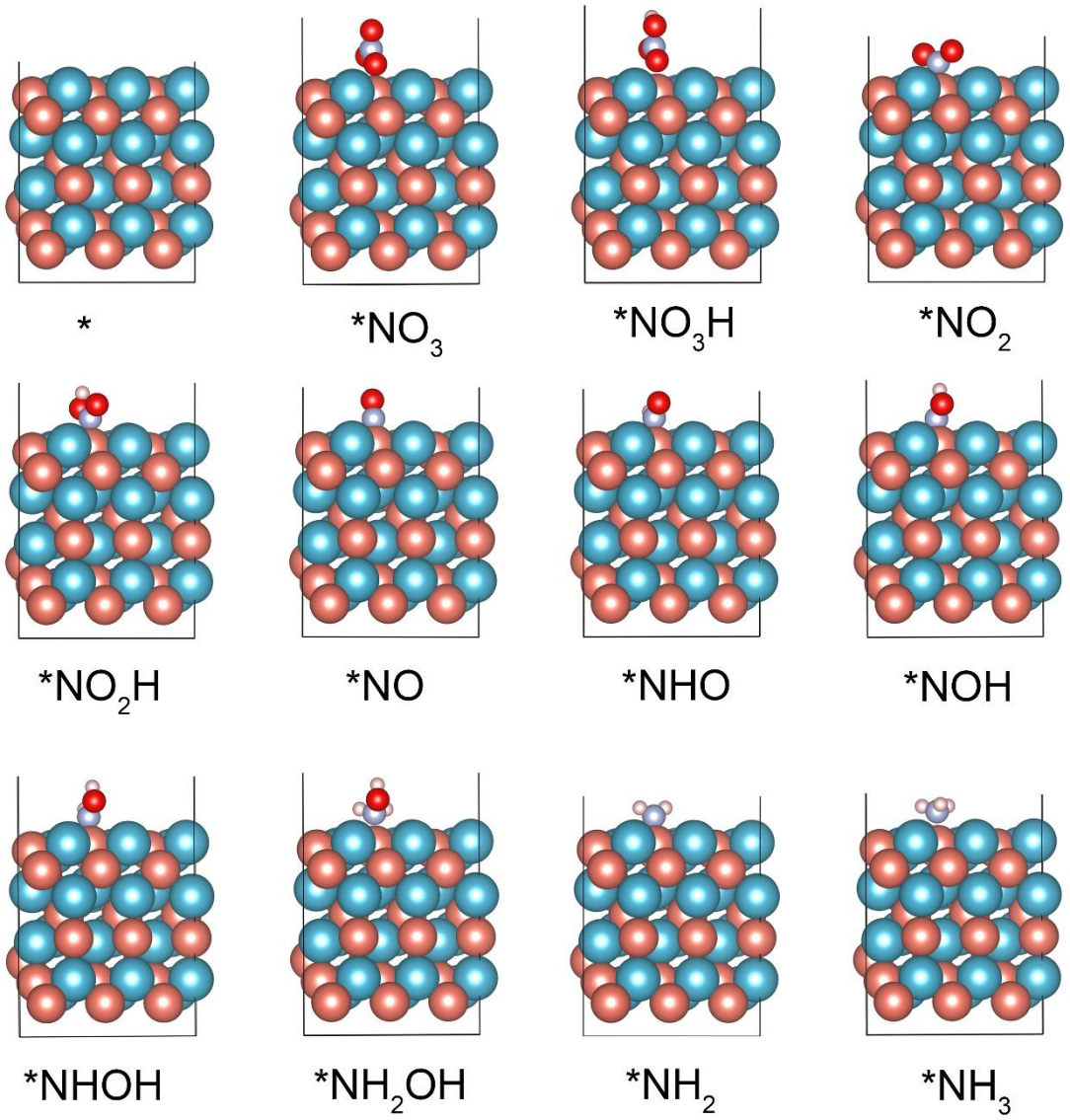

Supplementary Fig. 38 | Optimized structural models of reaction intermediates for NO_3RR on CoSb (101).

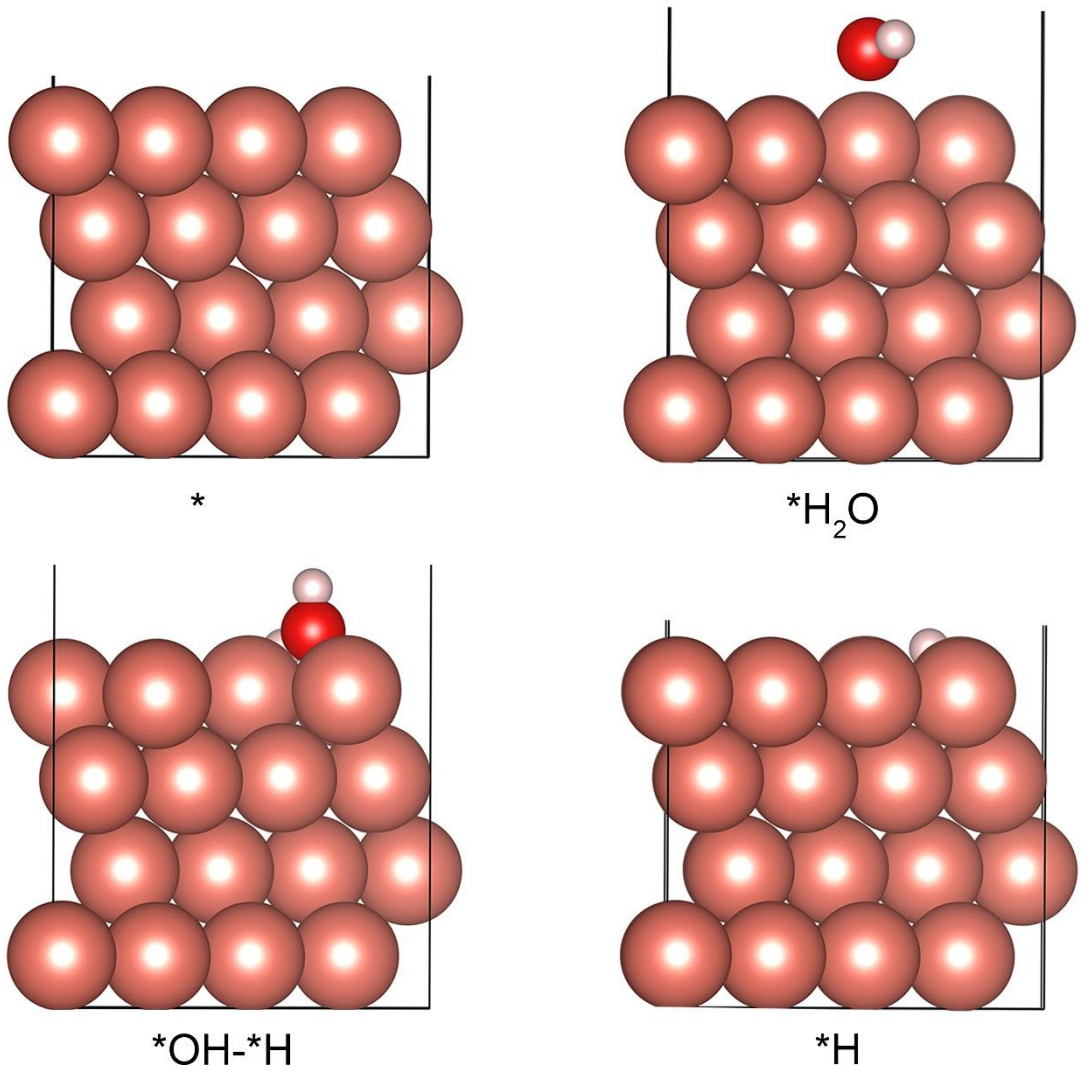

Supplementary Fig. 39 | Optimized structural models in water dissociation and hydrogen formation processes on Co (111).

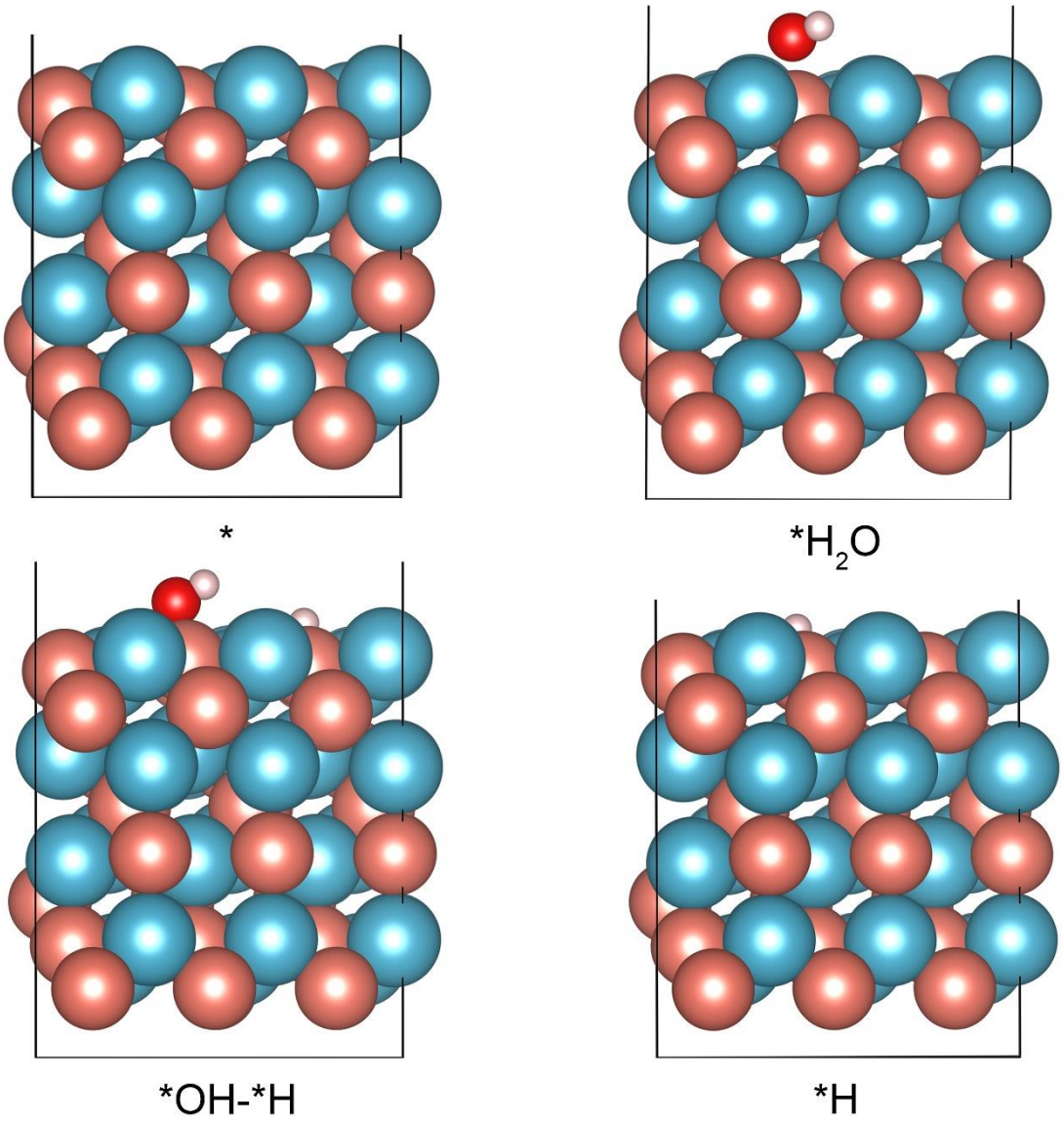

Supplementary Fig. 40 | Optimized structural models in water dissociation and hydrogen formation processes on CoSb (101).

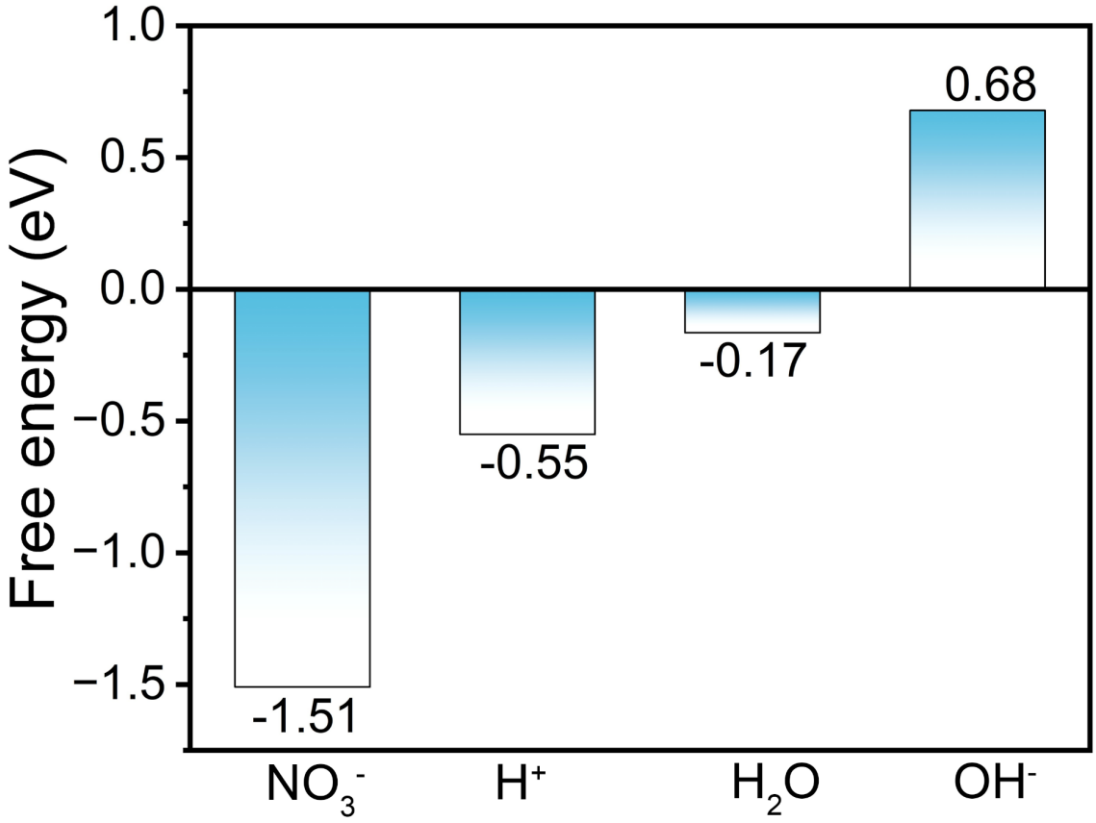

Supplementary Fig. 41 | The adsorption free energy of NO_3^-, H^+, H_2O and OH^- over CoSb (101).

Supplementary Tables

Supplementary Table 1 | ICP-OES results of CoSb IMCs/C and Co NPs/C.

Catalysts	Co (wt.%)	Sb (wt.%)	Co/Sb (at.%)
CoSb IMC/C	10.21	20.37	50.88:49.12
Co NPs/C	10.23	N/A	N/A

Supplementary Table 2 | EXAFS fitting at the Co and Sb K-edges for CoSb IMCs/C.

Sample	Path	CN	R (Å)	σ^2 (10^{-3}Å^2)	ΔE_0 (eV)	R factor (%)
Co K-edge	Co-Sb	6.0±0.2	2.53 ± 0.01	3.2	-0.9±0.6	0.005
	Co-O/C	3.8±0.8	2.02 ± 0.02	21.1	-0.9±0.6	
Sb K-edge	Sb-Co	5.8±0.2	2.73 ± 0.02	4.8	14.2 ± 2.2	0.018

CN is the coordination number; R is the interatomic distance (the bond length between central atoms and surrounding coordination atoms); σ^2 is the Debye-Waller factor (a measure of thermal and static disorder in absorber-scatter distances); ΔE_0 is the edge-energy shift (the difference between the zero kinetic energy value of the sample and that of the theoretical model). R factor is used to value the goodness of the fitting.

Supplementary Table 3 | Comparison of catalytic performance of CoSb IMCs/C with recently reported NO_3RR electrocatalysts

Catalyst	Electrolyte	NH_3 yield	NH_3 FE	Ref.
CoSb IMCs/C	**0.1 M KOH** **500 ppm NO_3^--N**	**4.92** mg h^{-1} cm^{-2}	**96.3%**	**This work**
O-Cu-PTCDA	0.1 M PBS 500 ppm NO_3^-	0.44 mg h^{-1} cm^{-2}	85.9%	*Nat. Energy* **2022,** 5, 605
Cu-N-C SAC	0.1 M KOH 1400 ppm NO_3^--N	4.50 mg h^{-1} cm^{-2}	84.7%	*J.Am.Chem.Soc.* **2022,** 144, 12062
Fe/Ni_2P	0.2 M K_2SO_4 700 ppm NO_3^--N	4.17 mg h^{-1} cm^{-2}	94.3%	*Adv Energy Mater.* **2022,** 12, 2103872
Ru_1Cu_{10}/rGO	1 M KOH 1400 ppm NO_3^--N	6.46 mg h^{-1} cm^{-2}	98%	*Adv. Mater.* **2023**, 35, 2202952
TiO_{2-x}	0.5 M Na_2SO_4 50 ppm NO_3^-	0.76 mg h^{-1} cm^{-2}	85.0%	*ACS Catal.* **2020**, 10, 3533-3540
Cu/Cu_2O NWAs	0.5 M Na_2SO_4 200 ppm NO_3^--N	4.16 mg h^{-1} cm^{-2}	95.8%	*Angew. Chem. Int. Ed.* **2020**, 59, 5350
NiPr-TPA-COF	0.5 M K_2SO_4 1400 ppm NO_3^--N	2.50 mg h^{-1} cm^{-2}	90%	*Energy Environ. Sci.* **2023**, 16, 201
PR-CuNC	0.1 M KOH 1400 ppm NO_3^--N	3.74 mg h^{-1} cm^{-2}	94.6%	*Appl. Catal. B* **2024**, 340,123228
Pd/TiO_2	0.5 M NaOH 3500 ppm NO_3^--N	1.12 mg h^{-1} cm^{-2}	92.0%	*Energy Environ Sci.* **2021**, 14, 3938
CoNi-V_p-1.0	0.5 M Na_2SO_4 50 ppm NO_3^--N	1.66 mg h^{-1} cm^{-2}	84.3%	*Appl. Catal. B* **2023**, 330, 1226271
$CoMn_2O_4$/NC	0.1 M Na_2SO_4 1400 ppm NO_3^--N	1.04 mg h^{-1} cm^{-2}	92.4%	*Appl. Catal. B* **2023**, 322,122090
Co-Fe@Fe2O3	0.1 M Na_2SO_4 500 ppm NO_3^--N	0.88 mg h^{-1} cm^{-2}	85.2%	*Proc. Natl. Acad. Sci. USA.* **2022**, 119, e2115504119
Co-CNP	0.02 M Na_2SO_4 100 ppm NO_3^--N	0.43 mg h^{-1} cm^{-2}	92.0%	*Proc. Natl. Acad. Sci. USA.* **2022**, 119, e2123450119
Fe_2TiO_5	PBS 140 ppm NO_3^--N	12.41 mg h^{-1} mg^{-1}	87.6%	*Angew. Chem. Int. Ed* **2023,** 62, e2022157

Supplementary References

1. Zhu, D., Zhang, L., Ruther, R.E., and Hamers, R.J. Photo-illuminated diamond as a solid-state source of solvated electrons in water for nitrogen reduction. *Nat. Mater*. **12**, 836-841 (2013).
2. Watt, G.W. and Chrisp, J.D. Spectrophotometric method for determination of hydrazine. *Anal Chem*. **24**, 2006-2008 (1952).
3. Kresse G., Furthmüller J. Efficient iterative schemes for ab initio total-energy calculations using a plane-wave basis set. *Phys. Rev. B* **54**, 11169-11186 (1996).
4. Perdew J. P., Burke K., Ernzerhof M. Generalized gradient approximation made simple. *Phys. Rev. Lett*. **77**, 3865-3868 (1996).
5. Blöchl P. E. Projector augmented-wave method. *Phys. Rev. B* **50**, 17953-17979 (1994).
6. Klimeš J., Bowler D. R., Michaelides A. Van der Waals density functionals applied to solids. *Phys. Rev. B* **83**, 195131 (2011).
7. Grimme S., Antony J., Ehrlich S., Krieg H. A consistent and accurate ab initio parametrization of density functional dispersion correction (DFT-D) for the 94 elements H-Pu. *J. Chem. Phys*. **132**, 154104 (2010).